8 Cooperative Spacecraft Formation Flying: Model Predictive Control with Open- and Closed-Loop Robustness

Louis Breger, Gokhan Inalhan, Michael Tillerson, and Jonathan P. How
Aerospace Controls Laboratory, Massachusetts Institute of Technology

Contents

8.1 Introduction

Formation flying of multiple spacecraft is an enabling technology for many future space science missions including enhanced stellar optical interferometers and virtual platforms for Earth observations [1, 2]. Controlling a formation will require several considerations beyond those of a single spacecraft. Key among these is the increased emphasis on fuel savings for a fleet of vehicles because the spacecraft must typically be kept in an accurate formation for periods on the order of hours or days [3–5], and the performance of the formation should degrade gracefully as one or more of the spacecraft runs out of fuel [6]. This chapter presents a model predictive controller that is particularly well-suited to formation flying spacecraft because it explicitly minimizes fuel use, exploits the well-known orbital dynamics environment, and naturally incorporates constraints (e.g., thrust limits, error boxes). This controller is implemented using Linear Programming (LP) optimization, which can be solved very rapidly and has always-feasible formulations. The resulting algorithms can be solved in real-time to optimize fuel use and are sufficiently robust that they can be embedded within an autonomous control system.

Efficient execution of precise formation flying relies on both accurate descriptions of the fleet dynamics and accurate knowledge of the relative states. Navigational errors [7, 8] and inaccurate physical models (such as ignored non-linearities, thruster misalignments, and differential disturbances such as J_2 and drag) can be significant sources of error [9].

Even though an open-loop analysis can model and numerically predict the impact of navigation and modeling errors on the fuel usage, there still remains the challenge of designing a control systems to produce fuel efficient and robust command inputs when subject to these errors. This chapter focuses on techniques to robustify the formation flying control system to handle these types of errors.

Our treatment of the control system design begins with the development of dynamic models in Section 8.2. In this section, starting from the general nonlinear model, we present the linearized dynamics for relative motion around a circular and eccentric orbit. In addition, a survey of dynamics used in formation flight literature, extensions to cases with disturbances and the new directions such as Gauss Variational Equations (GVEs) are reviewed. Section 8.3 provides a survey of recent control techniques used in formation flying; a more extensive survey on the state-of-art in formation flying is provided in Refs. [10, 11]. The last part of Section 8.3 covers the basics of the model predictive controller (MPC) developed in our previous work [12], and provides the mathematical basis for the formation flying control algorithms for multiple spacecraft. This mathematical formulation provides the flexibility of enabling state constraints, disturbance and sensor noise models, and actuator limitations. In addition, the formulation is directly applicable to a variety of linearized discrete dynamics matrices, such as the ones obtained via approximation methods [13], direct integration [14], and closed-form solutions [15]. In this work, the controller proposed in Ref. [12] is used as a baseline design and is modified to address formation-wide cooperation and robust formation keeping aspects of fuel critical missions.

With these goals in mind, the fourth section presents a new coordination method, *virtual center* which enables the model predictive controllers on each satellite to cooperate to achieve formation wide fuel savings [16]. The virtual center represents the weighted average motion of the fleet, including an average of the predicted disturbances. Since the formation tracking through the virtual center results in each spacecraft using its control effort against the disturbances relative to the fleet average, the weights in the average can be updated to balance the fuel usage across the fleet. This approach is compared to the widely used leader–follower coordination mechanism, and the results demonstrate formation-wide fuel savings. However, even though fleet coordination provides a balanced mission execution, the accuracy of this execution relies on path planning that is robust to disturbances and sensor noise. Thus, it is crucial to devise robust planning methods within the cooperation structure to enable formation flight for extended periods of time under realistic disturbances and sensor noise.

The final two sections provide two complementary approaches to achieve this objective: open-loop control objective selection and closed-loop robust planning. Section 8.5 examines the effect of changing the terminal condition of the formation keeping optimization to include both the original robust error-box constraint and also a requirement that the spacecraft nominally enter a closed orbit inside the error box. This method, called the *control objective selection approach* [17], is shown to be effective at reducing the frequency of replanning required by the controller. The last section presents an alternate form of robustness that guarantees that the spacecraft will remain inside an error box, and explicitly accounts for the possibility of future feedback. This *closed-loop robustness*

approach [17], is shown to be less conservative than requiring that the initial planned trajectory robustly remain inside the error box without replanning.

Finally, the three major developments are combined to create a hierarchical fleet-optimal control system that uses periodic terminal conditions, closed-loop robustness, and virtual-center coordination. The performance of this system is demonstrated in a fully non-linear formation flying simulation.

8.2 Dynamics of formation flight

The performance of any controller design depends on the fidelity of the embedded system dynamics model. This section presents the dynamics for the relative motion of a satellite with respect to a reference satellite (or a reference point) on an eccentric orbit. Even though these orbital dynamics are well known, its highly non-linear form complicate the development of precise control laws and online optimization algorithms. To simplify the dynamics for analysis and control, it is common to linearize with respect to the separation distance between satellites in the formation. A common set of linearized dynamics for circular orbits is Hill's Equations of Motion [18]. For elliptical orbits, linearizations are typically parameter-varying [19–21], where the parameter is the reference orbit true anomaly. This transition to linearized dynamics in case of short baseline separations for circular and eccentric Keplerian reference orbits is especially useful in modeling multiple spacecraft control and coordination problems. In the last part of this section, we summarize various extensions to these equations in order to account for disturbances. Our brief but precise development of the formation flight equations of motion follows Ref. [21], and the full details are available from classical texts such as Refs. [19, 22, 23].

The location of each spacecraft within a formation can be given by

$$\vec{R}_j = \vec{R}_{fc} + \vec{\rho}_j \tag{8.1}$$

where $\vec{R}_{fc}$ and $\vec{\rho}_j$ correspond to the location of the formation center and the relative position of the j^{th} spacecraft with respect to that point. The choice of formation center is rather arbitrary and can either be fixed to an orbiting satellite, or just be chosen as a local point that provides a convenient reference for linearization and development of linear control laws. The reference orbit in the Earth Centered Inertial (ECI) reference frame is represented by the standard orbital elements $(a, e, i, \Omega, \omega, \theta)$, which correspond to the semi-major axis, eccentricity, inclination, right ascension of the ascending node, argument of periapsis and true anomaly.

With the assumption that $|\vec{\rho}_j| \ll |\vec{R}_{fc}|$, the equations of motion of the j^{th} spacecraft under the gravitational attraction of a main body

$${}_i\ddot{\vec{R}}_j = -\frac{\mu}{|\vec{R}_j|^3}\vec{R}_j + \vec{f}_j \tag{8.2}$$

can be linearized around the formation center to give

$${}_i\ddot{\vec{\rho}}_j = -\frac{\mu}{|\vec{R}_{fc}|^3}\left(\vec{\rho}_j - \frac{3\vec{R}_{fc}\cdot\vec{\rho}_j}{|\vec{R}_{fc}|^2}\vec{R}_{fc}\right) + \vec{f}_j, \tag{8.3}$$

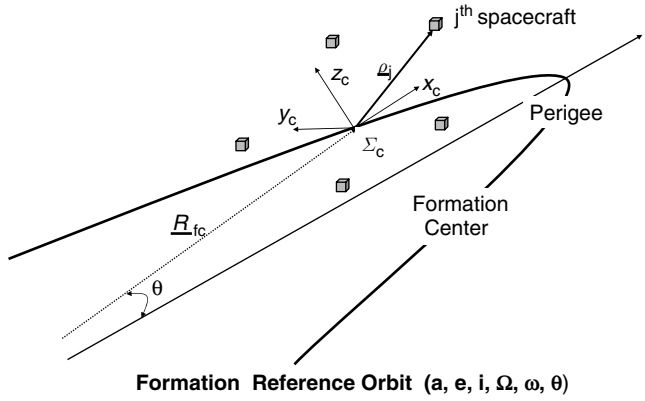

Fig. 8.1. Spacecraft formation.

where the accelerations associated with other attraction fields, disturbances or control inputs are included in $\vec{f}_j$. The derivatives in the ECI reference frame are identified by the preceding subscript i. A natural basis for inertial measurements and scientific observations is the orbiting (*non-inertial*) reference frame Σ_c, fixed to the formation center (see Figure 8.1). Using kinematics, the relative acceleration observed in the inertial reference frame ${}_i\ddot{\vec{\rho}}_j$ can be related to the measurements in the orbiting reference frame

$${}_i\ddot{\vec{\rho}}_j = {}_c\ddot{\vec{\rho}}_j + 2{}_i\dot{\vec{\Theta}} \times {}_c\dot{\vec{\rho}}_j + {}_i\dot{\vec{\Theta}} \times ({}_i\dot{\vec{\Theta}} \times \vec{\rho}_j) + ({}_i\ddot{\vec{\Theta}} \times \vec{\rho}_j), \tag{8.4}$$

where ${}_i\dot{\vec{\Theta}}$ and ${}_i\ddot{\vec{\Theta}}$ correspond to the angular velocity and acceleration of this orbiting reference frame. The fundamental vectors $(\vec{\rho}_j, \vec{R}_{fc}, {}_i\vec{\Theta})$ in Eqs. (8.3) and (8.4) can be expressed in Σ_c as

$$\vec{\rho}_j = x_j\hat{k}_x + y_j\hat{k}_y + z_j\hat{k}_z \tag{8.5}$$

$$\vec{R}_{fc} = R_{fc}\hat{k}_x \tag{8.6}$$

$$i\dot{\vec{\Theta}} = \dot{\theta}\hat{k}_z, \tag{8.7}$$

where the unit vector $\hat{k}_x$ points radially outward from Earth's center (anti-nadir pointing) and $\hat{k}_y$ is in the in-track direction along increasing true anomaly. This right-handed reference frame is completed with $\hat{k}_z$, pointing in the cross-track direction. All of the proceeding vectors and their time rate of changes are expressed in the orbiting reference frame Σ_c.

Combining Eqs. (8.3) and (8.4) to obtain an expression for ${}_c\ddot{\vec{\rho}}_j$, and using Eqs. (8.5)–(8.7), it is clear that the linearized relative dynamics with respect to an eccentric orbit can be expressed via a unique set of elements and their time rate of change. This set consists of the relative states $[x_j, y_j, z_j]$ of each satellite, the radius R_{fc} and the angular velocity $\dot{\theta}$ of the formation center. Using fundamental orbital mechanics describing

planetary motion [24, 25], the radius and angular velocity of the formation center can be written as

$$|\vec{R}_{fc}| = \frac{a(1-e^2)}{1+e\cos\theta}, \quad \text{and} \quad \dot{\theta} = \frac{n(1+e\cos\theta)^2}{(1-e^2)^{3/2}}, \tag{8.8}$$

where $n = \sqrt{\mu/a^3}$ is the natural frequency of the reference orbit. These expressions can be substituted into the equation for ${}_c\ddot{\vec{\rho}}_j$ to obtain the relative motion of the j^{th} satellite in the orbiting formation reference frame. The first correct formulation of the below equations in its original form is attributed to Lawden [19].

$$\begin{aligned}\frac{\mathrm{d}}{\mathrm{d}t}\begin{bmatrix}\dot{x}\\ \dot{y}\\ \dot{z}\end{bmatrix}_j = &-2\begin{bmatrix}0 & -\dot{\theta} & 0\\ \dot{\theta} & 0 & 0\\ 0 & 0 & 0\end{bmatrix}\begin{bmatrix}\dot{x}\\ \dot{y}\\ \dot{z}\end{bmatrix}_j - \begin{bmatrix}-\dot{\theta}^2 & 0 & 0\\ 0 & -\dot{\theta}^2 & 0\\ 0 & 0 & 0\end{bmatrix}\begin{bmatrix}x\\ y\\ z\end{bmatrix}_j - \begin{bmatrix}0 & -\ddot{\theta} & 0\\ \ddot{\theta} & 0 & 0\\ 0 & 0 & 0\end{bmatrix}\begin{bmatrix}x\\ y\\ z\end{bmatrix}_j\\ &+n^2\left(\frac{1+e\cos\theta}{1-e^2}\right)^3\begin{bmatrix}2x\\ -y\\ -z\end{bmatrix}_j + \begin{bmatrix}f_x\\ f_y\\ f_z\end{bmatrix}_j.\end{aligned} \tag{8.9}$$

The terms on the right-hand side of this equation correspond to the Coriolis acceleration, centripetal acceleration, accelerating rotation of the reference frame, and the virtual gravity gradient terms with respect to the formation reference. The right-hand side also includes the combination of other external and control accelerations in $\vec{f}_j$. These terms can be explicitly presented for each spacecraft as

$$\begin{bmatrix}f_x\\ f_y\\ f_z\end{bmatrix}_j = \begin{bmatrix}u_x\\ u_y\\ u_z\end{bmatrix}_j + \begin{bmatrix}w_x\\ w_y\\ w_z\end{bmatrix}_j \tag{8.10}$$

where $u = [u_x(t)\ u_y(t)\ u_z(t)]^T : \mathbb{R} \to \mathbb{R}^3$ represents the control inputs and

$$w = [w_x(t)\ w_y(t)\ w_z(t)]^T : \mathbb{R} \to \mathbb{R}^3$$

represents the combination of other external accelerations, such as disturbances. Note that care must be taken when interpreting and using the equations of motion and the relative states in a non-linear analysis. The difficulty results from the linearization process, which maps the curvilinear space to a rectangular one via a small curvature approximation. In this case, a relative separation in the in-track direction in the linearized equations actually corresponds to an incremental phase difference in true anomaly, θ.

For a circular reference orbit, $e = 0$, substituting $\dot{\theta} = n_o$, $\ddot{\theta} = 0$, and the well known Clohessy–Wiltshire or Hill's equations are

$$\begin{aligned}\frac{\mathrm{d}}{\mathrm{d}t}\begin{bmatrix}\dot{x}\\ x\\ \dot{y}\\ y\\ \dot{z}\\ z\end{bmatrix} = &\begin{bmatrix}0 & 3n_o^2 & 2n_o & 0 & 0 & 0\\ 1 & 0 & 0 & 0 & 0 & 0\\ -2n_o & 0 & 0 & 0 & 0 & 0\\ 0 & 0 & 1 & 0 & 0 & 0\\ 0 & 0 & 0 & 0 & 0 & -n_o^2\\ 0 & 0 & 0 & 0 & 1 & 0\end{bmatrix}\begin{bmatrix}\dot{x}\\ x\\ \dot{y}\\ y\\ \dot{z}\\ z\end{bmatrix} + \begin{bmatrix}1 & 0 & 0\\ 0 & 0 & 0\\ 0 & 1 & 0\\ 0 & 0 & 0\\ 0 & 0 & 1\\ 0 & 0 & 0\end{bmatrix}\begin{bmatrix}u_x\\ u_y\\ u_z\end{bmatrix} + \begin{bmatrix}1 & 0 & 0\\ 0 & 0 & 0\\ 0 & 1 & 0\\ 0 & 0 & 0\\ 0 & 0 & 1\\ 0 & 0 & 0\end{bmatrix}\begin{bmatrix}w_x\\ w_y\\ w_z\end{bmatrix}\end{aligned} \tag{8.11}$$

Numerical experience have shown that the applicability of Hill's equations to various formation flying maneuvers is limited to strictly circular orbits and short baseline separations on the order of 1 m to 1 km. However, transforming in-track separations to relative anomaly angles (rectangular map of curvilinear space), allows for larger baseline formation initialization and formation-keeping maneuvers.

8.2.1 Extensions to formation flight dynamic representations

Linearized relative orbital dynamics equations of motion of the type discussed in this chapter typically rely on several key assumptions: small vehicle separations ($\rho/R \ll 1$) and Keplerian motion. They ignore the non-Keplerian effects of drag and J_2[1] and some (e.g., Hill's equations) also assume no reference orbit eccentricity. In recent years, a number of new dynamics models have been published that capture the effects of these disturbances. Table 8.1 summarizes the dynamics models that have been commonly used for formation-flight control.

The inherent inability of Hill's equations to account for the eccentricity of the Keplerian reference orbit provides a dominant source of error, even for typical STS mission eccentricities such as $e = 0.005$. In comparison, Lawden's equations [19, 21] provide the flexibility to account for reference orbit eccentricities up to $e = 0.8$. Similar to Hill's equations, the applicability of these equations is also limited by the non-linearity introduced with large vehicle separations. The addition of second and third order non-linearity effects [27, 29, 31] provides better approximations for larger vehicle separations. These non-linearity corrections are, however, limited to circular reference orbits and degrade rapidly with larger eccentricity. The Ref. [26] modifies Hill's equations to include differential J_2 effects.

Differential orbital elements [22, 30] and Gauss' Variational Equations (GVE) [15, 23, 32, 33] can be used to simultaneously account for large baselines, reference eccentricity, and J_2 effects [28, 33]. The linearized GVE approach in Ref. [33] uses slowly changing differential orbital elements that are linearized about the desired orbit of each spacecraft in the spacecraft formation. Linearization error then grows with the state error of each

Table 8.1
The matrix of formation-flight dynamics used for control and the corrections introduced by the corresponding authors.

	$e = 0$ no J_2	$0 < e < 1$ no J_2	$e = 0$ with J_2	$0 < e < 1$ with J_2
Linearized dynamics	Hill's [18]	Lawden [19] Inalhan [21]	Schweighart [26]	
Long baseline capable	Karlgrad [27] Mitchell [29] Alfriend [31]	GVEs [23] Alfriend [30]	Gim [28]	Gim [28] Breger [33]

[1] J_2 is the major correction term to uniform gravitational attraction because of Earth's oblateness.

spacecraft rather than the overall size of the formation. As in the case of Lawden's equations, the linearized GVEs in Ref. [33] are linear parameter-varying (LPV), making them particularly well-suited to use within the model predictive control presented in this chapter.

The next section reviews the techniques available for formation flight control and develops a model predictive controller using one of the linearized dynamics presented in this section.

8.3 Formation flight control and the model predictive control formulation

The goal of formation flying control is for several vehicles to create and maintain a desired formation utilizing the limited resources available on each spacecraft while acting as a single system. In this context, we can divide this specific control task into two distinct parts. First is the *formation initialization and keeping* which initializes the desired formation to a passive aperture[2] and maintains it against disturbances. Second is the *formation planning* which creates trajectories for the formation to follow during maneuvers such as reshaping or retargeting of the formation. The primary focus of the formation flying control research to date has been to develop fuel efficient methods of performing these two distinct tasks. For formation planning and keeping, many formation control approaches have been suggested in recent years spanning a large range of control techniques, including PD, LQR, LMI, nonlinear, Lyapunov, impulsive, and model predictive control [12, 34–41].

For formation initialization and keeping, typically it is assumed that a formation is initialized to a passive aperture and deviations caused by disturbances such as differential drag and/or differential J_2 is corrected through feedback laws. Passive apertures, created through slight differences in eccentricity, inclination, and argument of latitude, provide a natural structure for formation initialization. These apertures inherently take advantage of the orbital dynamics of the spacecraft in the absence of disturbance forces to create a periodic relative motion through establishing no-drift conditions which set zero differential energy across the fleet [21, 42, 43]. The size, shape and the relative initial conditions for these passive apertures is designed by using the closed-form solutions for the non-linear or the linearized orbital equations. This idea can be further extended to mitigate the effects of the disturbances, such as J_2, by establishing initial conditions [43] which results in zero average relative drifts in special orbits. However, when such special orbit selection is not available, it is necessary to develop control laws for keeping spacecraft in formation.

Control law approaches, such as Lyapunov and PD controllers [37], require that control be applied continuously, a strategy both prone to high fuel use and difficult to implement when thrusting requires attitude adjustment. Other approaches, such as the impulsive thrusting scheme introduced in Ref. [44], require spacecraft to thrust at previously specified times and directions in the orbit, ensuring that some of the maneuvers will not be fuel-optimal. Many of the non-linear feedback control schemes available in literature [10]

[2] Passive apertures are typically short baseline periodic formation configurations that provide good, distributed, Earth imaging and reduce the tendency of the vehicles to drift apart.

utilize feedback linearization, wherein control commands are used to cancel the nonlinear dynamics and replace them with linear dynamics that are typically not the natural dynamics of an orbiting satellite. The linearized relative dynamics discussed in the previous section also provide many avenues for control development. For example, numerous linear quadratic regulators have been developed that force a vehicle to track a desired state [45–47]. However, these feedback control schemes require almost constant control effort which leads to high fuel costs over the length of a mission. In order to reduce fuel costs, recent research has focused on developing methods to generate fuel-time optimal control sequences over a period of time rather than just one step.

This section presents a method of determining fuel/time optimal control inputs and trajectories using linear programming (LP), which was first introduced in Ref. [12]. This LP formulation is the base of the control work presented in this chapter. Linear programming solves for the minimum fuel maneuver explicitly by minimizing a sum of the control inputs for the solution over a given planning horizon. The general formulation can include any form of linearized dynamics and disturbance models. The LP formulation also provides a general framework for including various types of state and actuator constraints. LP can be used for different types of maneuvers: formation maneuvers, individual station-keeping, formation-keeping, or general trajectory planning. Note that this type of control system, in addition to providing an optimal planning algorithm, replaces a reactive control system when used as a feedback controller. In literature, this technique is known as *model predictive control* (MPC) [48]. Figure 8.2 shows the MPC algorithm that each spacecraft in the formation implements.

To develop a model predictive controller for formation flight[3], we consider the general set of linear time-varying (LTV) continuous equations of motion

$$\dot{x}(t) = A(t)x(t) + B(t)u(t) + B_d(t)w(t), \tag{8.12}$$

which can be used to describe the relative dynamics of each satellite with respect to a reference Keplerian orbit. Here $x(t) \in \mathbb{R}^n$ are the states, $u(t) \in \mathbb{R}^m$ are control inputs, $w(t) \in \mathbb{R}^p$ are differential disturbances. Note that, in what follows, the dynamics could

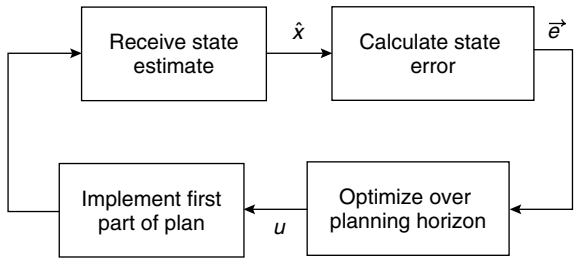

Fig. 8.2. Algorithm followed by each spacecraft in the formation.

[3] The technique developed in this section is independent of different techniques that can be used for discretization of system dynamics.

have be written as a linear parameter-varying (LPV) model, where the parameter is the true anomaly of the reference orbit, as is the case for Lawden's equations [19, 12], by using Kepler's equation to determine the true anomaly as a function of time [23]. There are a number of ways to develop discrete dynamics for optimization: approximation methods [13], direct integration [14] or closed-form solutions [15]. A straightforward, yet computationally intensive approach, is to numerically integrate the A and B matrices to obtain the discrete dynamics [49] using the following identify

$$\frac{\mathrm{d}}{\mathrm{d}t}\Phi(t, t_0) = A(t)\Phi(t, t_0)\ \forall t, \quad \Phi(t_0, t_0) = I, \tag{8.13}$$

where $\Phi(t, t_0)$ is the state transition matrix from a time t_0 to time t. In some cases, Φ can be found by solving the equations of motion directly, or by using the fundamental solution matrix [15, 50], which corresponds to the homogenous solution to Eq. (8.13). This matrix is represented by F_k for a specific time interval

$$F_k = \Phi((k+1)T_s, kT_s), \tag{8.14}$$

where T_s is the duration of a time step and k corresponds to the k^{th} step in the discretization. The discrete input matrix G_k is given by

$$G_k = \int_{kT_s}^{(k+1)T_s} \Phi((k+1)T_s, \tau)B(\tau)\mathrm{d}\tau \tag{8.15}$$

using a zero-order hold (ZOH) assumption on the input. The ZOH assumption is appropriate for periods of thrusting that are significant relative to the duration of a time step. Equation (8.15) can be accurately computed using direct integration, but this is typically computationally expensive for online implementation. If the equations of motion are linear time invariant (LTI), or if the time step is sufficiently short that the parameter can be considered constant between discretization points, then F_k and G_k take the form [51]

$$F_k = e^{A_k T_s}, \quad G_k = \int_{kT_s}^{(k+1)T_s} e^{A_k \tau}\mathrm{d}\tau B_k, \tag{8.16}$$

where A_k and B_k are the constant state transition and input matrices for the interval $((k+1)T_s, kT_s)$. The approximate forms of F_k and G_k in Eq. (8.16) are significantly less expensive to compute than the direct integration in Eq. (8.15), but any integration errors must be carefully monitored to determine their effect on the closed-loop performance. Note that if, instead, the thrusting occurs quickly relative to the duration of a time step, then the input can be assumed to be impulsive, and $G_k = B(kT_s)$ [51]. A similar analysis must also be performed for the disturbance input matrix, M_k, which is calculated using the disturbance input matrix B_{dk}.

Using any of these discretization options, the discrete dynamics take the following form

$$x(k+1) = F_k x(k) + G_k u(k) + M_k w(k), \quad t = kT_s. \tag{8.17}$$

For any given k^{th} time step, the variables of interest $z(k) \in \mathbb{R}^l$ can be extracted from the states $x(k)$ and input variables $u(k)$ as

$$z(k) = H_k x(k) + J_k u(k), \quad t = kT_s, \tag{8.18}$$

where H_k and J_k correspond to output matrices for the optimization. The result $z(k)$ can be explicitly written as a function of the input variables $u(1), \ldots, u(k-1)$ up to the k^{th} step, initial state $x(0)$, and the discrete system dynamics using the convolution sum [49]

$$z(k) = H_k F^{(k,k)} x(0) + J_k u(k) + \sum_{i=0}^{k-1} H_k F^{(k-i-1,k)} \left[G_i u(i) + M_i w(i) \right] \quad k \geq 1, \tag{8.19}$$

where $F^{(j,k)}$ corresponds to

$$F^{(j,k)} = \begin{cases} F_{(k-1)} \cdots F_{(k-j+1)} F_{(k-j)} & 2 \leq j \leq k \\ F_{(k-1)} & j = 1 \\ I & j = 0 \end{cases}. \tag{8.20}$$

Further, Eq. (8.19) can be structured into a compact matrix representation

$$z(k) = \Gamma(k) U_k + h(k), \tag{8.21}$$

where

$$\Gamma(k) = \left[\begin{array}{cccc} H_k F^{(k-1,k)} G_0 & H_k F^{(k-2,k)} G_1 & \ldots & H_k F^{(0,k)} G_{k-1} \quad J_k \end{array} \right] \tag{8.22}$$

and

$$h(k) = \left[\begin{array}{cccc} H_k F^{(k-1,k)} M_0 & H_k F^{(k-2,k)} M_1 & \ldots & H_k F^{(0,k)} M_{k-1} \end{array} \right] \begin{bmatrix} w(0) \\ w(1) \\ \vdots \\ w(k-1) \end{bmatrix} + H_k F^{(k,k)} x(0) \tag{8.23}$$

and the input vector is

$$\mathrm{U}_k = \left[\begin{array}{cccc} u(0)^T & u(1)^T & \ldots & \ldots u(k-1)^T \quad u(k)^T \end{array} \right]^T \tag{8.24}$$

The disturbance inputs $w(k)$ are used to account for *known* dynamics that are not modeled in the A_k matrices. For example, Hill's dynamics do not model aerodynamic drag, however equations describing these effects are readily found in the literature [52]. By calculating the effects of drag on each satellite at each time step a priori, these effects can be included in the optimization. By including known disturbances on the dynamics, the controller is better able to prevent constraint violations and conserve fuel in cases where the disturbance acts as required input would have.

This affine plant description is the basis of the formation keeping control problem. The objective of each vehicle in this problem is to minimize fuel use

$$J = \min_{U_n} \sum_{j=1}^{m} c_j \| u(j) \|_1, \tag{8.25}$$

where c_j terms are scalar weights. Note that the 1-norm is used as the fuel use metric, because it correctly identifies the velocity change costs (ΔV) for spacecraft with axial thrusters. The vehicles are constrained to maintain their state to within some tolerance of

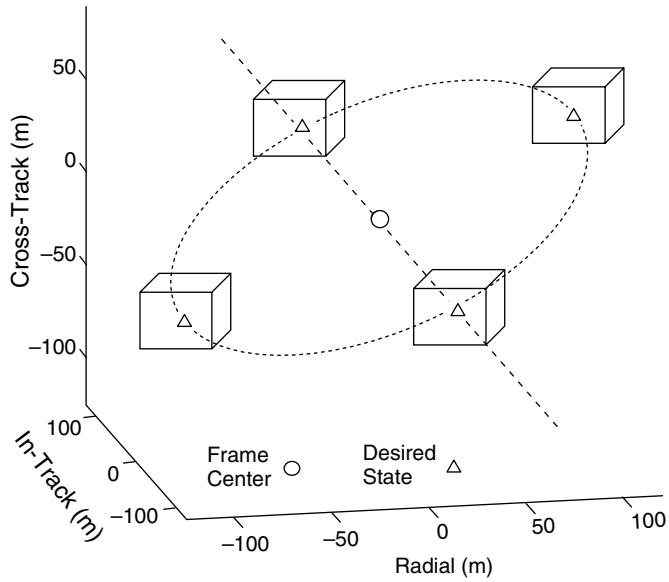

Fig. 8.3. Error boxes and desired states for a formation in a relative frame centered around a reference orbit.

a specified desired set of coordinates at each time-step k. These state constraints create an "error-box" around the desired state of the spacecraft (see Figure 8.3). Using an error box has advantages over tracking a desired point: it is more fuel efficient, better captures the mission constraints, and allows "breathing room" for the controller to account for modeling errors. The performance specification at each step k is

$$a|z_j(k) - z_{j_{\text{des}}}(k)| \leq z_{\text{tol}\,j}, \quad z_{\text{tol}\,j} \geq 0 \tag{8.26}$$

$$\Rightarrow \; -z_{\text{tol}\,j} \leq z_j(k) - z_{j_{\text{des}}}(k) \leq z_{\text{tol}\,j} \qquad \forall\; j = 1, \ldots, l \tag{8.27}$$

where $z_{\text{tol}\,j}$ is the error bound associated with each coordinate z_j. The vector $z_{\text{des}}(k)$ is the *desired state* at step k and has the same dimensions as z. The resulting MPC optimization uses the cost function from Eq. (8.25) and the constraints from Eq. (8.27).

The one-norm cost function used in the linear program (LP) is formulated by splitting the input matrix into positive, U_n^+, and negative, U_n^-, parts that are recombined after optimization

$$U_n = U_n^+ - U_n^-, \quad U_n^+ \geq 0, \; U_n^- \geq 0 \tag{8.28}$$

which gives the cost function

$$J^* = \min_{U_n^+, U_n^-} \begin{bmatrix} C^T & C^T \end{bmatrix} \begin{bmatrix} U_n^+ \\ U_n^- \end{bmatrix}, \tag{8.29}$$

where $C^T = [c_0, \ldots, c_n]$. Constraints on the maximum input can be imposed using

$$\begin{bmatrix} I & 0 \\ 0 & I \end{bmatrix} \begin{bmatrix} U_n^+ \\ U_n^- \end{bmatrix} \leq \begin{bmatrix} u_{\max} \\ u_{\max} \end{bmatrix}, \tag{8.30}$$

where $u_{\max}$ is the maximum thruster input. A variety of additional practical constraints are described in Ref. [12]. The constraints on spacecraft state at each step k are then written

$$\begin{bmatrix} \Gamma(k) & -\Gamma(k) \\ -\Gamma(k) & \Gamma(k) \end{bmatrix} \begin{bmatrix} U_k^+ \\ U_k^- \end{bmatrix} \leq \begin{bmatrix} z_{\text{des}}(k) - h(k) + z_{\text{tol}} \\ -z_{\text{des}}(k) + h(k) + z_{\text{tol}} \end{bmatrix} \quad \forall\, k \in \{1 \ldots n\} \tag{8.31}$$

$$\begin{bmatrix} -I & 0 \\ 0 & -I \end{bmatrix} \begin{bmatrix} U_n^+ \\ U_n^- \end{bmatrix} \leq \begin{bmatrix} 0 \\ 0 \end{bmatrix} \tag{8.32}$$

in order to ensure that the spacecraft remains inside an error box centered on a desired state (Eq. (8.31)) and that elements of U_n^+ and U_n^- are optimized to be positive (Eq. (8.32)). Note that the constraint matrices and vectors here can be compiled in a single large set of constraints

$$\mathbf{A}\hat{U} \leq \mathbf{b}, \tag{8.33}$$

where $\hat{U}$ is the concatenation of U_k^+ and U_k^-, and $\mathbf{A}$ and $\mathbf{b}$ capture the constraints at all steps k considered in the optimization.

Remark 8.3.1. One method to achieve robustness to unmodeled disturbance and noise terms is to identify the worst-case disturbance sequence that would force the spacecraft out of the desired error boxes. One way of approximating this is to find the disturbance sequence, w_{um}^*, that would result in total maximum variation in the spacecraft states of interest. Assuming that the unmodeled terms are set bounded (such as $|w(k)| \leq w_{\max}(k)$, for convenient LP formulation), this problem can be formulated using the convolution step in Eq. (8.22)

$$w_{um}^* = \arg \max_{[w(0), \ldots, w(m-1)]} \sum_{k=0}^{m-1} z_{um}(k) \tag{8.34}$$

$$\text{subject to } z_{um}(k) = \begin{bmatrix} H_k F^{(k-1,k)} M_0 & H_k F^{(k-2,k)} M_1 & \ldots & H_k F^{(0,k)} M_{k-1} \end{bmatrix} \begin{bmatrix} w(0) \\ w(1) \\ \vdots \\ w(k-1) \end{bmatrix}$$

$$z_{um}(k) \geq 0$$

$$|w(k)| \leq w_{\max}(k), \quad \forall k = 0, \ldots, m-1.$$

Define z_{um}^* as the value of $z_{um}(k)$ for w_{um}^*, then the error box tolerance constraints in the original LP formulation (i.e., Eq. (8.27)) can be modified through $z_{tol}^{new}(k) = z_{tol}^{old} - z_{um}^*(k)$.

Thus, at any time step, the constraints are contracted to account for the unmodeled worst-case disturbance sequence that could force them out of the errors boxes in a given time horizon, m. If the LP formulation is used as an open-loop feedback loop using replanning, then distinct parts of the time horizon can be emphasized by introducing weights to states in the cost function: $\sum_{k=0}^{m-1} c_{um}(k) z_{um}(k)$.

Remark 8.3.2. Error box constraints sometimes arise from the requirement that spacecraft achieve their desired states to within 10% of the formation separation [53]. Also, some missions would require that the error box be enforced at all times to achieve continuous observations [53], and others would only impose the constraint for brief periods during each orbit [54]. The constraints in Eq. (8.32) easily handle these cases through the addition or subtraction of steps k to the optimization, thereby enforcing the error box constraints at all times or only specific times.

Remark 8.3.3. This optimization problem is readily formulated as a linear program. Linear programming is a very fast optimization method that uses a linear, convex cost function and linear, convex constraints [55]. Linear programming was used for the simulation examples in this chapter, and in all cases required no more than a small fraction of a second to solve on a 3 GHz computer. Likewise, formulating the dynamics matrices used in the linear programs never required more than 10 seconds of computation time.

The center of each error box is referenced to the formation center, which could be a set of reference orbital elements or another spacecraft. The choices of the formation center are discussed in detail in the following section.

8.4 Distributed coordination through virtual center

Section 8.3 presented a model predictive controller that minimizes the fuel use and guarantees that the spacecraft will remain within an error box. However, a typical formation has multiple spacecraft that must all be constrained not to drift, and for some missions, form or maintain a particular shape. Thus the relative state requirements for the entire formation must be specified with respect to some reference point. This section investigates the effect of three different methods of specifying this reference point. The first is a point on a reference orbit that is propagated with the fleet. The second is a traditional *leader–follower*, where a leader is the formation reference point. The third approach involves a new method, called the *virtual center* [16, 56], which uses measurements taken by the spacecraft to calculate the location of the center. The virtual center approach is similar to the formation feedback method presented in Ref. [35], but is applied to spacecraft formation flying in low Earth orbit and explicitly uses a fuel weighting in the center calculation to equalize fuel use across the fleet. Another distinction is that the calculation of the virtual center is based on measurements available from the relative navigation estimator developed for this application [57, 58]. Using the virtual center extends the previous *formation-keeping control* in Section 8.3 to *formation flying control* by enabling extensive cooperation between the vehicles. At the end of this section, we compare these

three approaches through simulation and show that the virtual center method results in fleet-wide fuel savings and fuel balance across the formation.

Remark 8.4.1. Desired states relative to the reference point are specified using passive apertures designed with the closed-form solutions to various linearized equations of relative motion [21, 42, 43]. Passive apertures are designed to result in drift-free motion, but disturbances such as differential drag cause the formation to disperse, necessitating feedback control. Our approach uses a control algorithm based on linear programming (LP) to minimize fuel cost (see Section 8.3).

8.4.1 Reference point coordination

One of the first steps in applying the LP technique for a spacecraft control system is to determine the *desired state*, which is the current state in the desired trajectory for the spacecraft. An error box is fixed to the desired state to provide a position tolerance for the satellite. A key point in this section is that the error box is specified relative to a desired point for the spacecraft. This section investigates various techniques for specifying the desired points for the formation, and demonstrates how any error in the spacecraft location relative to the current desired point can be estimated using the onboard carrier-phase differential GPS (CDGPS) measurements [58].

The formation-keeping LP algorithm in Section 8.3 is formulated to control a single spacecraft to maintain a desired state to within some tolerance specified by an error box. The formation-keeping algorithm is applied independently to each spacecraft, which enables the required computation to be distributed across the fleet. The desired state for each spacecraft is specified relative to a *reference point*, which can be chosen to enable *cooperation* between the spacecraft in the fleet, thereby enabling true formation flying.

Figure 8.4 depicts a typical scenario for a formation of three spacecraft, in which the desired trajectories of the spacecraft have been designed to create a projected ellipse in a relative frame [59]. This type of formation is known as a passive aperture and has a size determined by the formation radius. The formation angle is measured from maximum positive radial displacement. The initial conditions and closed-form solutions to the relative dynamics are used (with the drift-free constraints imposed [21]) to find the desired states at future times. The desired state is specified relative to the formation center, which is determined relative to a *formation reference point*. Three methods for determining the reference point are discussed in the following subsections. Each method is evaluated for its complexity and the amount of information flow required for its execution.

8.4.1.1 Reference orbit

A simple method of specifying the reference point is using the reference orbit. The reference orbit is a point in space that is propagated using a model that describes the average fleet orbit. The formation center is attached to the reference orbit and is used to specify the desired spacecraft states. The reference point is described by the non-linear orbit equations, requiring little communication between vehicles. Also note that the

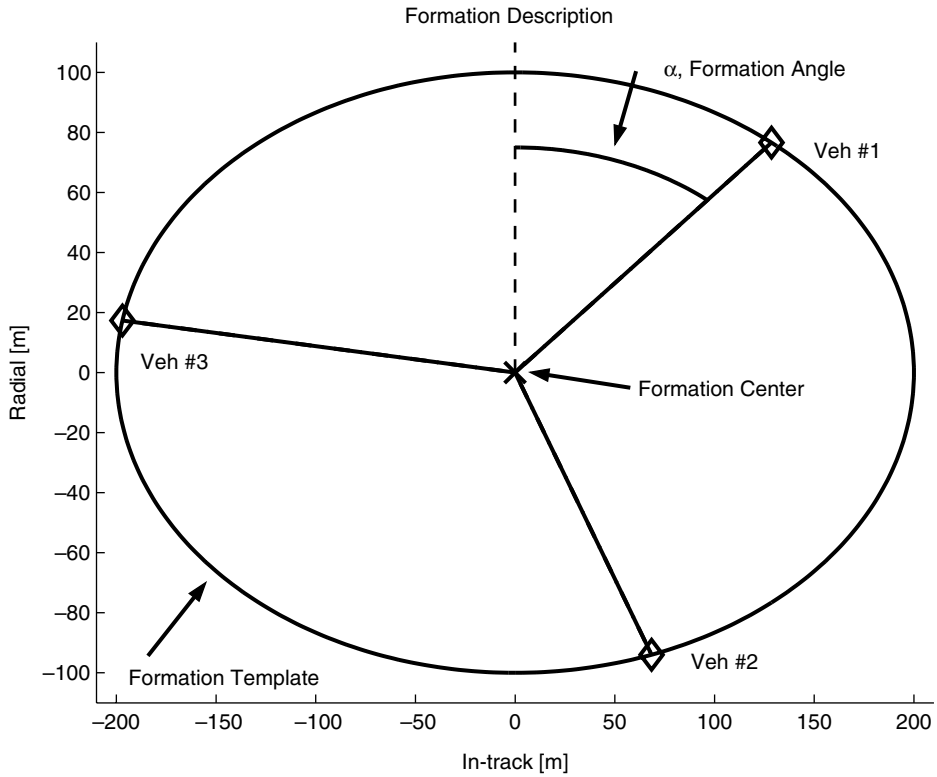

Fig. 8.4. The formation geometry is described relative to the formation center, marked by a $\times$. Each vehicle state is specified by a radius and an angle.

reference point is not specified using measurements, so there is no uncertainty in the state due to sensor noise. A disadvantage of this approach is that the reference point does not naturally experience the fleet disturbances. Instead, a disturbance model must be included in the propagation. If the model is inaccurate, the fleet will track a reference orbit that does not describe the fleet motion. Instead of using control effort to maintain the fleet, effort would be wasted "chasing" a mathematical point in space that does not move with the fleet.

8.4.1.2 Leader–follower

Another common method of specifying the reference point is to let a vehicle be the *leader* and fix the reference point to the leader spacecraft. The advantage is that the reference point is on a spacecraft, which eliminates the need to propagate the motion and it naturally captures the absolute disturbances. The leader–follower method requires little information flow, because the reference state is just the state of the leader spacecraft.

One leader–follower configuration places the leader at the aperture center, but this makes it prohibitively expensive to change leaders in the formation. Alternately, the leader spacecraft could be one of the vehicles on the passive aperture. The desired state for each follower spacecraft then becomes the desired state for the follower relative to the aperture center minus the desired state of the leader from the aperture center. This simplifies the transition between leaders, because no maneuvers are required. However, instantaneously switching leaders could cause a jump in the desired state of each spacecraft and must be done with care.

A disadvantage of this method is that the leader does not represent the average fleet motion, forcing some followers to overcome larger disturbances than others. Also, the leader spacecraft will use minimal fuel, because its state never experiences error. To equalize control effort across the fleet, the leader spacecraft can be alternated based on the fuel usage/status within the fleet.

8.4.1.3 Virtual center

An alternative approach to reference orbit and leader–follower tracking is to use a "virtual center" as the reference point. The reference state in this case is estimated using measurements between the spacecraft in the fleet. An advantage of the virtual center is that it represents the weighted average motion of the fleet, including an average of the actual disturbances. The weighted average enables cooperation within the fleet. The virtual center method presented here is similar to the formation feedback method for multiple vehicle control presented in Ref. [35], but our approach differs, because we show how the virtual center can be implemented using sensors planned for formation flying missions [57, 58]. The navigation algorithm presented in Ref. [57] uses decentralized estimators to filter the CDGPS measurements, precisely determining the location of each spacecraft relative to a reference vehicle. The following discussion assumes that the reference vehicle is the leader, but that is not necessary in general. Given the estimated states relative to the leader, it is possible to precisely determine the formation center.

Figure 8.5 shows a formation of three spacecraft. The thick solid lines are known or measurable distances. The thin solid lines represent the true distances to the virtual center, which are compared to the specified desired state relative to the virtual center (dashed lines). To calculate the relative position and velocity of the center, a measurement reference state must be specified. In the figure, the reference frame is attached to spacecraft #1, which will be referred to as the reference spacecraft. Inter-spacecraft states, $\vec{x}_{1i}$, are measured relative to the reference spacecraft and are represented by the solid lines in Figure 8.5. The virtual center state, $\vec{x}_c$, is also specified relative to the reference spacecraft. Each spacecraft state relative to the virtual center is

$$\vec{x}_{ci} = \vec{x}_{1i} - \vec{x}_c. \tag{8.35}$$

The error states are the difference between the state of each spacecraft relative to the center, x_{ci}, and the desired state for that spacecraft, which is also specified relative to the center. Error states in the figure are the differences between the $\Diamond$ and $\circ$ for each spacecraft.

$$\vec{x}_{ci} - \vec{x}_{i,des} = \vec{e}_i. \tag{8.36}$$

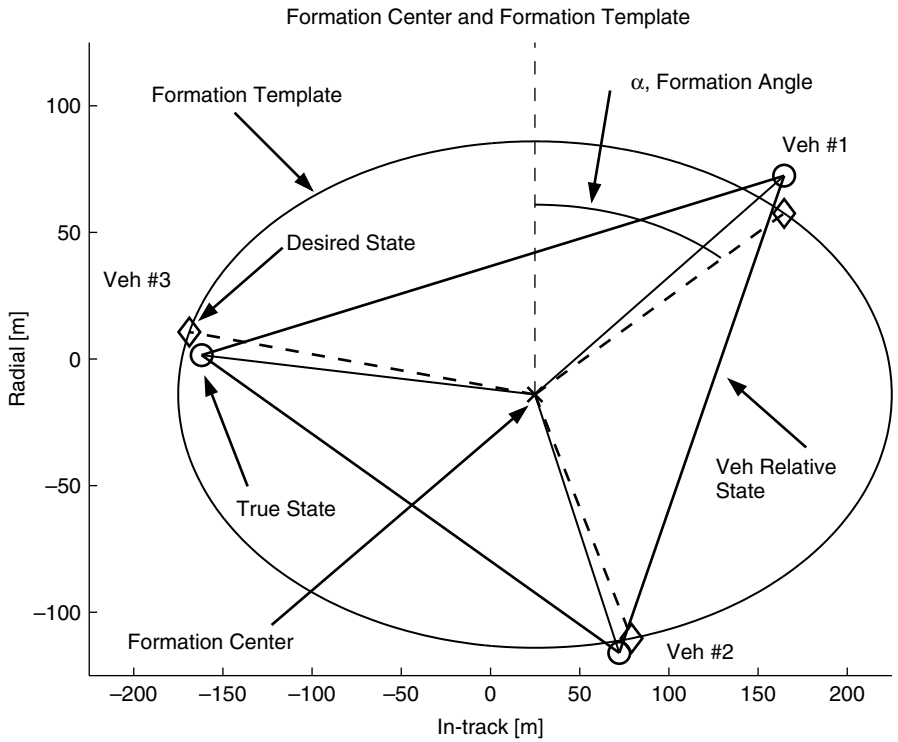

Fig. 8.5. Virtual center calculated from measured relative states (thick solid) and used to determine desired states (dashed) and actual state (thin solid) of each spacecraft.

Substituting Eq. (8.35) for x_{ci} yields the following expression for the vehicle error in terms of known quantities and the unknown virtual center, $\vec{x}_c$,

$$\vec{x}_{1i} - \vec{x}_c - \vec{x}_{i,des} = \vec{e}_i. \tag{8.37}$$

The error equation for each spacecraft becomes

$$\begin{bmatrix} \vec{x}_{11} - \vec{x}_{1,des} \\ \vec{x}_{12} - \vec{x}_{2,des} \\ \vdots \\ \vec{x}_{1N} - \vec{x}_{N,des} \end{bmatrix} - \begin{bmatrix} I \\ I \\ \vdots \\ I \end{bmatrix} \left[\vec{x}_c\right] = \begin{bmatrix} \vec{e}_1 \\ \vec{e}_2 \\ \vdots \\ \vec{e}_N \end{bmatrix} \equiv \vec{e} \tag{8.38}$$

which can be compactly rewritten as

$$b_c - A_c x = \vec{e}. \tag{8.39}$$

The virtual center location $\vec{x}_c$, is chosen to minimize the sum of the errors, $\|\vec{e}\|_2 = (b_c - A_c x)^T (b_c - A_c x)$. A weighting matrix, W, can be included to increase the importance of a

vehicle or state, giving the weighted least-squares problem $\min(b_c - A_c x)^T W(b_c - A_c x)$, with solution

$$\hat{x}_c = \left(A_c^T W A_c\right)^{-1} A_c^T W b_c. \tag{8.40}$$

Note that using the normalized current fuel consumption in the weighting matrix allows fuel use across the fleet to be equalized over time.

Remark 8.4.2. Given the special form of b_c and A_c the calculation of the virtual center can be decentralized using the following algorithm

$$\hat{x}_{c_1} = b_1, \tag{8.41}$$

$$\hat{x}_{c_i} = \hat{x}_{c_{i-1}} + \frac{w_i}{\bar{w}_{i-1} + w_i}(b_i - \hat{x}_{c_{i-1}}), \tag{8.42}$$

where $b_i = \vec{x}_{1i} - \vec{x}_{i,\mathrm{des}}$, w_i is the weight of the i^{th} estimate, and $\bar{w}_i = \sum_{j=1}^{i} w_j$. In this formulation, spacecraft i passes its current state estimate, $\hat{x}_{c_i}$ and the scalar $\bar{w}_i$ to spacecraft $i+1$ to update the estimate of the optimal center position. The error-minimizing fuel-weighted virtual center can be computed in one cycle around a formation. The final estimate can then be shared with the rest of the fleet.

Using the virtual center method, updates can be made to the virtual center state every time step or periodically with a propagation of the virtual state between updates. A key advantage of this method is that the disturbances affecting each spacecraft become differential disturbances relative to the fleet average, which will lower fuel costs. Measuring spacecraft error relative to a regularly updating virtual center makes the absolute motion of the fleet unobservable to individual spacecraft. Thus, absolute motion will not enter into the LP, ensuring control effort is only utilized for relative geometry maintenance. A disadvantage is that the virtual center calculation must be centralized, since the current and desired states of all spacecraft must be collected in one place to find the virtual center, requiring an increase in communication throughout the fleet. Also, noise and uncertainty in measurements will lead to uncertainty in the virtual center state.

A further issue with this approach is that the virtual center is a function of the states of all the vehicles in the fleet, so any control effort by one vehicle will influence all of the other vehicles. When a vehicle uses a control input to correct an error, the control input assumes the virtual center is fixed over the plan horizon. However, the location of the center will change over time as each vehicle moves. The control inputs from the other vehicles can be included in this decentralized control algorithm by having all vehicles "publish" a list of planned control actions and then having each vehicle include the inputs of the other vehicles as *disturbance inputs* into their dynamics. The control inputs get scaled to give the motion for the virtual center in the near future. Unfortunately, there is no guarantee the published plans will get fully implemented, which may cause errors in the trajectory design.

Another way to predict the effect of external control inputs on the virtual center is to form a centralized LP to solve for all vehicles' control inputs simultaneously. The virtual center state at each time step is described in terms of the vehicle states, as in

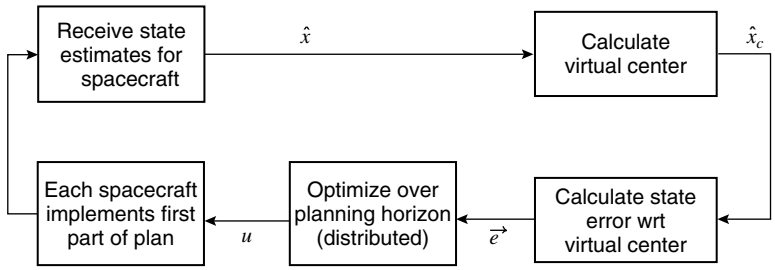

Fig. 8.6. Algorithm for model predictive control with virtual center coordination. Note that the calculation of the virtual center can be decentralized and the plan optimization step occurs concurrently for all spacecraft in the formation.

Eq. (8.40), capturing the center motion due to all control inputs. Control input solutions and trajectories would then have to be sent to each vehicle, increasing the communication load, thereby making this approach intractable for larger fleets. Figure 8.6 shows an updated version of the MPC algorithm (see Figure 8.2) that includes the virtual center calculation.

8.4.2 Simulations results

Several simulations were performed to demonstrate the effectiveness of the new coordination method. FreeFlyer™ [60] orbit simulation software is used as the nonlinear propagator for each satellite while MATLAB™ mathematical software is used to implement the controller. The entire control system is executed without human intervention.

The simulation consists of three vehicles, each modeled as a 45 kg Orion spacecraft [57] with different drag coefficients (2.36, 2.20, and 2.12). Other disturbances, such as gravity perturbations, solar radiation pressure, atmospheric lift, and third body effects are activated in the FreeFlyer™ propagator. Sensor noise is included in the simulation as a white noise component added to the true relative state. The magnitude of the sensor noise is bounded by 2 cm for position and 0.5 mm/s for velocity, based on expected CDGPS sensor noise [57]. Spacecraft thrusters provide a maximum acceleration of 0.003 m/s^2, which corresponds to continuous thrusting for a full time-step. The formation is initialized on a reference orbit (semi-major axis 6900 km, eccentricity of 0.005) similar to a space shuttle orbit. The reference orbit inclination is 35°, introducing significant differential gravity disturbances for spacecraft with inclination differences. See Ref. [56] for the full details on the simulation parameters.

When using the virtual center procedure, the reference point is updated at every time-step. The relative dynamics are discretized on a 10.8 second time interval to match the propagation step-size. Formation flying problems are planned over a half-orbit time horizon. The LP formation flying formulation restricts control inputs and applies position constraints to every sixth time-step [61], which reduces LP solution times to about 1–3 seconds. The robust LP approach in Ref. [7] is used to account for sensor noise and the always feasible approach in Ref. [61] is also used. The error box size for position

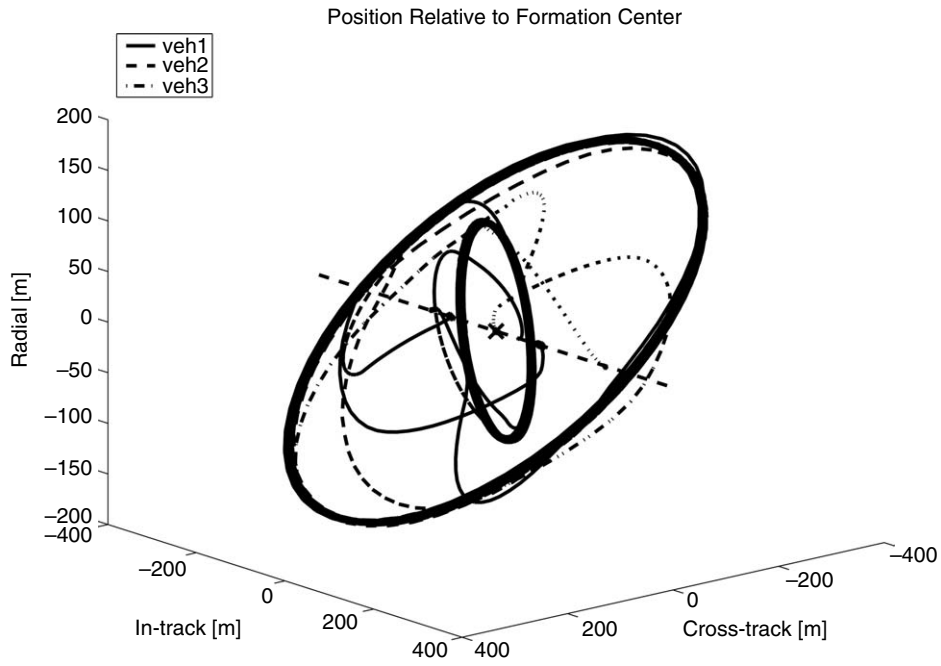

Fig. 8.7. Relative motion for three-vehicle formation. Sequence is in-track separation, small ellipse, larger ellipse, in-track separation.

tolerance is 10 m in-track, 5 m radial, and 5 m cross-track, which meets the tolerance requirement of 10% of the baseline for all formations in the simulation.

The simulation contains three formation maneuvers with formation flying at each configuration. The spacecraft paths during maneuvers are shown with respect to the virtual reference point in Figure 8.7. The formation begins and ends in similar in-track separations. Two passive aperture formations are maintained for approximately seven days each to observe any long- and short-term effects of the disturbances, particularly the gravity perturbation effects. The first aperture projects a 400×200 m ellipse in the in-track–radial plane and a circle with a 100 m radius in the radial–cross-track plane. The second aperture projects a 600×300 m ellipse in the in-track–radial plane and a 300 m radius circle in the in-track–cross-track plane. Aperture position assignment is coordinated through the procedure described in Section 8.3 with a plan horizon of one orbit.

8.4.2.1 Analysis of controller performance

Full simulation fuel costs for the leader–follower and fuel-weighted virtual center methods are shown in Figures 8.8 and 8.9. The fuel cost figures show three reconfiguration maneuvers, each of which uses a significant amount of fuel over a short period of time. The longer, constant slope segments correspond to the periods of formation-flying. Comparing the two figures, it is clear that the Leader–Follower method has a higher fuel

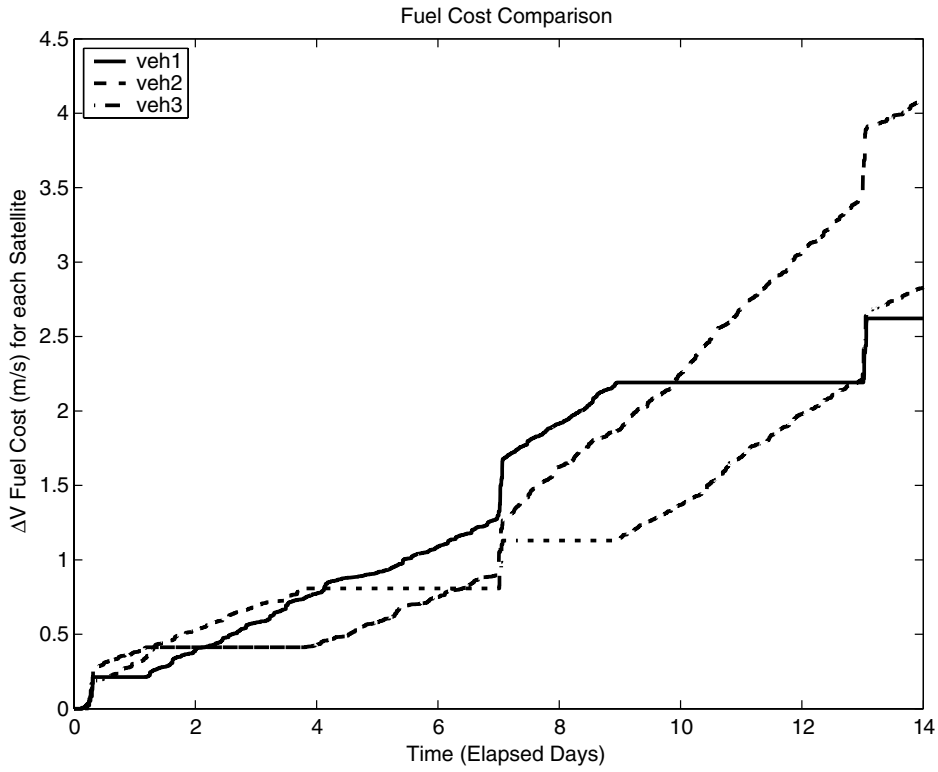

Fig. 8.8. ΔV's for each vehicle, using Leader–Follower—sharp rises indicate formation maneuvers and constant slope parts correspond to formation flying.

cost than the virtual center method throughout the mission. In the leader–follower figure, a spacecraft exerting no control (the flat lines) is presently the leader of the formation and, consequently, has no state error. When the total control effort exerted by one spacecraft significantly exceeds that of the other spacecraft, the leader is switched to balance overall fuel use. In comparison, the fuel-weighted virtual center method spreads the error out among all of the spacecraft, with the objective of placing the virtual center in such a way as to minimize global control effort across the formation. As a result, there is a non-zero fuel cost for all three spacecraft during the formation-flying mode.

The simulations using a virtual center reference point were performed for three different levels of fleet cooperation. The first simulation calculates the virtual center in the formation with equal weights on each vehicle in the fleet. The second simulation includes the control actions of other spacecraft in the control determination. The third simulation includes the external control inputs, as in the second simulation, and also adjusts the weighting of the vehicles based on fuel use. All three methods successfully achieve and maintain the specified configurations during the simulation. In the formation-flying mode, the vehicles are maintained approximately within the specified position tolerance due to the always-feasible formulation. The maximum deviation

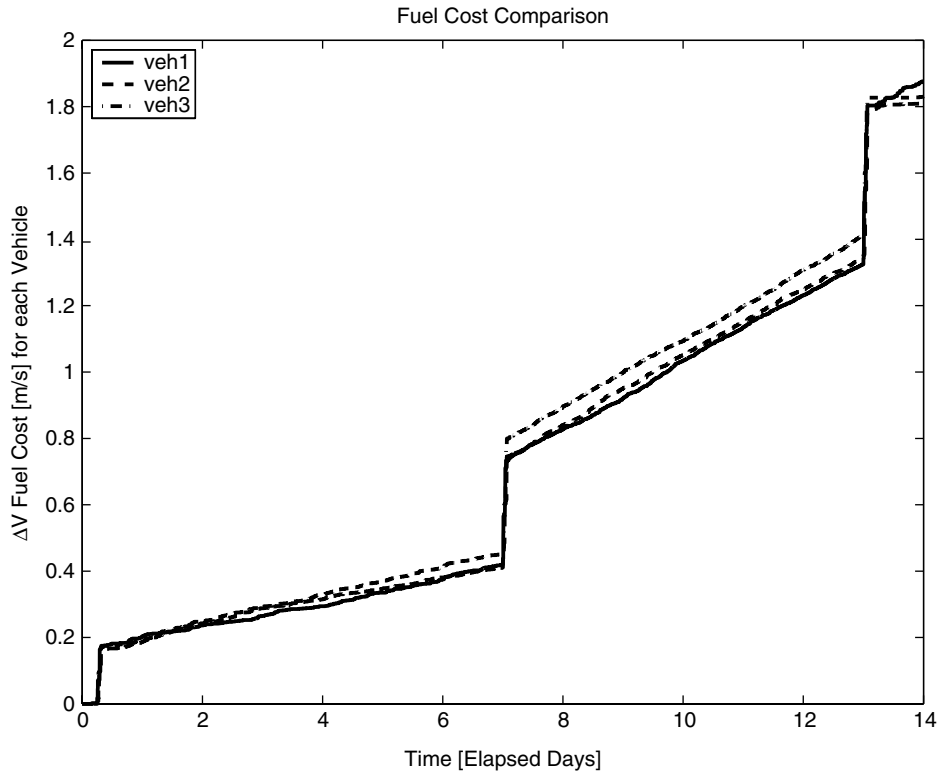

Fig. 8.9. ΔV's for each vehicle, using Virtual Center—sharp rises indicate formation maneuvers and constant slope parts correspond to formation flying. Note that the *y*-axis scale differs from that of Figure 8.8. The plots show that the Virtual Center method achieves both better fuel distribution across the fleet and better overall fuel minimization than the Leader–Follower method.

from the desired state for any simulation was less than 11 m in-track, 5 m radial, and 7 m cross-track. The total fuel cost data for each of the simulations is contained in Table 8.2.

8.4.2.2 Formation flying analysis—FM

The results in Table 8.2 show that there is no appreciable difference in fuel cost between the three different controllers for the formation maneuvers; however, this is not unexpected. The difference between the first two simulations is the inclusion of the control inputs of other vehicles in the low-level controller for formation-flying. Therefore, there is no expected improvement in the formation maneuvers from this change. The last simulation adds fuel weighting to the calculation of the formation center. The fuel weighting is only updated once every two orbits, whereas the formation maneuvers occur over a single orbit. Some benefit can be expected, because the fuel weighting will reduce

Table 8.2
Table of ΔV use for the virtual center simulations. Simulation number corresponds to level of coordination used. Spacecraft are indicated by number. The maneuver types are followed by the number of orbits the maneuver was performed for. FF indicates formation flying and FM represents formation maneuvers.

	Sim 1			Sim 2			Sim 3		
Maneuver type	SC 1	SC 2	SC 3	SC 1	SC 2	SC 3	SC 1	SC 2	SC 3
FF #1 (4) mm/s/orbit	0.509	0	0.523	0.652	0	0.112	0.542	0	0.341
FM #1 (1) mm/s	163	150	171	160	148	168	169	157	165
FF #2 (101) mm/s/orbit	3.07	2.82	2.43	2.70	2.54	2.26	2.39	2.48	2.51
FM #2 (1) mm/s	315	291	315	339	291	320	275	306	314
FF #3 (90) mm/s/orbit	8.14	6.90	6.18	7.42	6.57	6.59	6.59	6.73	6.82
FM #3 (1) mm/s	415	440	391	408	410	374	404	392	393
FF #4 (14) mm/s/orbit	2.64	4.69	2.30	1.71	0.696	1.45	3.90	2.25	0.541
FM Total (3) mm/s	893	881	877	907	849	862	848	855	872
FF Total (209) mm/s	1141	1040	899	1019	920	931	979	1004	964
Total Fuel (212) mm/s	2034	1921	1776	1926	1769	1793	1827	1859	1836

the differential disturbances of vehicles that have used large amounts of fuel, however, this change will be minimal over the course of one orbit.

8.4.2.3 Formation flying analysis—FF

For the two passive aperture formation flying maneuvers, the rate at which fuel is expended for each vehicle is heavily dependent on the cross-track disturbance. The in-track and radial control efforts are approximately equal for each vehicle in the formation, regardless of the spacecraft location in the aperture; however, the cross-track fuel use varies significantly for each vehicle. The cross-track disturbance results in a secular increase in the amplitude of the cross-track oscillatory motion, and the magnitude of this increase depends on the cross-track phasing. With a three vehicle formation, it is impossible to eliminate the disturbance completely for every vehicle, therefore, at least two vehicles will experience a cross-track disturbance and will expend more control effort than the other in response to the cross-track disturbance. Altering the phasing over time can equalize the average cross-track disturbance for all vehicles [45]. This method could be included in the control system in Section 8.3, but note that the coordinated virtual center equalizes the fuel cost due to the cross-track disturbance through the calculation of the fuel-weighted virtual center.

8.4.2.4 Total fuel cost analysis

The controllers can be compared by the total fuel cost for the mission. If a formation flying mission requires the entire fleet to perform the science observations, then the mission life will be limited by the vehicle with the greatest fuel use. The fuel expenditure for each vehicle during the mission is summarized in the last row of Table 8.2. The results show that the maximum fuel cost is reduced from 2.03 m/s for the first simulation to 1.93 m/s for the second simulation. However, the fuel cost for one vehicle is much larger

than for the other two vehicles in both simulations. The third simulation utilizes the fuel weighting method to reduce the maximum fuel use by shifting control effort to the lower fuel cost vehicles. The result is a reduction in the maximum fuel cost to 1.86 m/s.

8.4.3 Summary

This section addresses the three main issues of the formation flying coordination problem: the reference point for the formation, the specification of the desired state, and the control to achieve or maintain the desired state across the whole formation. The new virtual center method presents a procedure for calculating the reference point for the fleet from which the desired states for each spacecraft can be readily calculated. Note that the calculation of this virtual center is closely tied to the planned formation flying sensor (CDGPS in LEO). The selection of the location of the center also includes a weighting on fuel use across the fleet, which facilitates increased coordination and cooperation within the distributed model predictive control system. The result is an efficient real-time control system using the benefits of a fuel-optimal controller to plan control actions and coordination between the fleet to further reduce fuel effort. The simulation results indicate that this control system can adequately maintain a formation at a fuel cost of 2–8 mm/s per orbit. The simulations also clearly show that the virtual center approach required significantly less fuel than the leader–follower technique. In the next two sections, two distinct approaches to achieve disturbance and sensor noise robustness are presented.

8.5 Open-loop robust control and replan frequency

The model predictive control system described in Section 8.3 has many tunable parameters, such as error box size, planning horizon length, replan frequency, terminal condition, and robustness level. The closed-loop behavior of the control system and its performance level can be significantly altered by posing the optimization problem in different ways. However, since the control inputs are determined using online optimization, the best choice of these parameters is typically not obvious. The Ref. [62] analyzes formation flying model predictive control (MPC) mission parameters when a particular form of closed-loop robustness is used. Here, robustness refers to the ability of a controller to operate in the presence of navigation error and can be closed-loop, where feedback effects are exploited, or open-loop, where full trajectories can be implemented without additional feedback. In the case of the open-loop robustness method in Ref. [12], another approach to choosing control parameters is required. This section examines the effect of terminal conditions on replan frequency of the controller described in Section 8.3.

Section 8.3 presents an MPC approach where the implementation horizon was made variable and replanning was triggered by the vehicle approaching the edge of the error box. Using a variable implementation horizon with a problem that has disturbances and noise will result in a control system with an uncertain replan rate. An investigation of

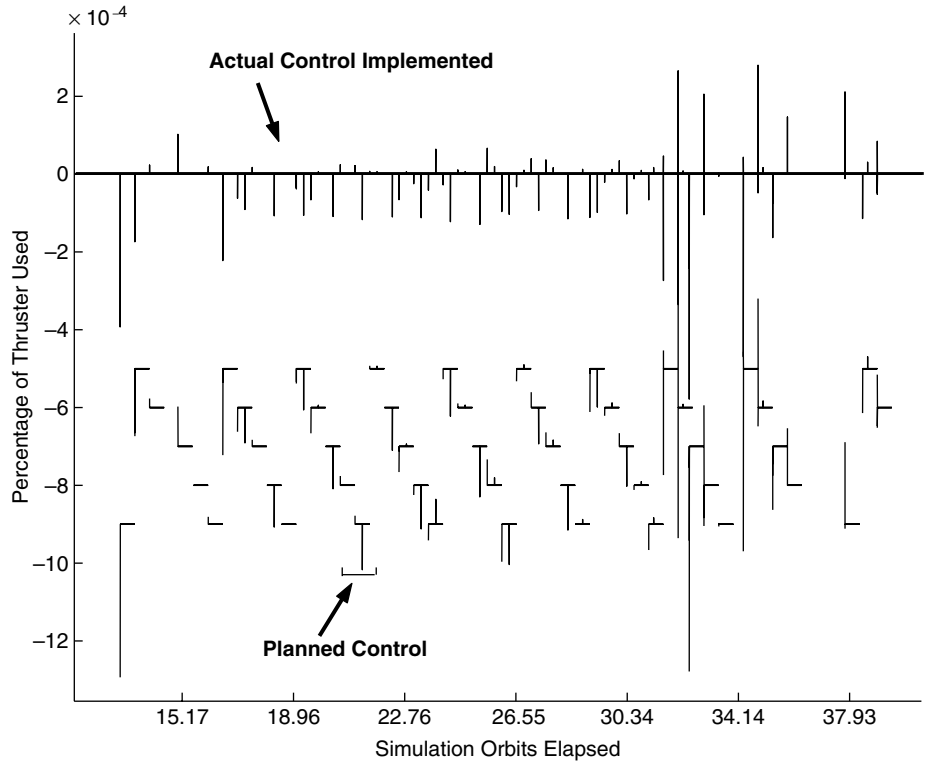

Fig. 8.10. Plans created using unmodified terminal conditions. The horizontal axis crossing the origin shows the thrusting that was implemented. The floating axes below the implementation axis indicate the planned thrusting sequence at time matching the far left side of each floating axis.

this controller showed that a replan was occurring at the end of each planning horizon. Figure 8.10 shows this phenomenon, where the actual control implemented (in thruster firings) is plotted along the x-axis and the plan being implemented at any given time is shown using floating axes in the lower half of the figure. Times when floating axes overlap indicate that a plan has been abandoned in favor of a new plan (i.e., a replan occurred). In this control formulation, the only event that can trigger a replan is a deadband violation. The figure shows that the majority of replans occur soon after previous plans have completed (as opposed to replanning before a plan has completed, or after a long period of drifting).

In a typical error-box problem with fixed terminal time, the optimal solution is known to be a "bang-off-bang," which applies control for a set period, then allows the system to evolve unperturbed, and then applies control for another set period. The solution of the online optimization problem should reproduce this optimal solution. However, a model predictive controller (MPC) that has solved for a single plan does not necessarily implement that entire plan. Instead, the controller implements only the first part of the

plan (the *implementation horizon*) and then computes a new plan (re-planning). With no disturbances and no sensing noise, only one plan needs to be computed. However, when process and sensing noise is included, frequent re-planning may be required.

The cause of the specific replan rate is the noise robustness formulation. The noise robustness formulation used in Ref. [12] guarantees that a plan will be feasible (i.e., remain inside the error box) for a range of possible initial conditions h_i. Here, n_{ic} initial conditions are chosen to capture the bounds of expected initial condition error and each is used to evaluate a different set of vectors $h_i(k)\ \forall\ k \in \{1 \ldots n\}$. This formulation uses the constraint

$$\begin{bmatrix} \Gamma(k) & -\Gamma(k) \\ -\Gamma(k) & \Gamma(k) \end{bmatrix} \begin{bmatrix} U_k^+ \\ U_k^- \end{bmatrix} \leq \begin{bmatrix} z_{\text{des}}(k) - h_i(k) + z_{\text{tol}} \\ -z_{\text{des}}(k) + h_i(k) + z_{\text{tol}} \end{bmatrix} \forall \begin{array}{l} k \in \{1 \ldots n\} \\ i \in \{1 \ldots n_{\text{ic}}\} \end{array} \tag{8.43}$$

$$\begin{bmatrix} -I & 0 \\ 0 & -I \end{bmatrix} \begin{bmatrix} U_n^+ \\ U_n^- \end{bmatrix} \leq \begin{bmatrix} 0 \\ 0 \end{bmatrix}. \tag{8.44}$$

Ref. [12] presents a method of solving an identical optimization using fewer constraints. This robustness technique tends to keep the spacecraft inside the deadband for the duration of the planning horizon, thus eliminating the need for the plan to be interrupted. However, at the end of the plan, the spacecraft is often left near the edge of an error box (allowing drift as far as possible tends to minimize fuel use) and therefore requires almost immediate replanning (see Figure 8.11).

Although the motion shown in Figure 8.11 is the optimal solution to the problem that was posed, it results in very regular (several times an orbit) low level thrusting to return the spacecraft to the deadband. This is not desirable for several reasons: incorrect thrusting (not modeled here) introduces error into the state estimate and it requires regular GN&C computation and communication. A preferable system would achieve similar or better fuel use, while allowing for long periods of drifting inside the deadband. Two approaches were identified to alter the replan rate.

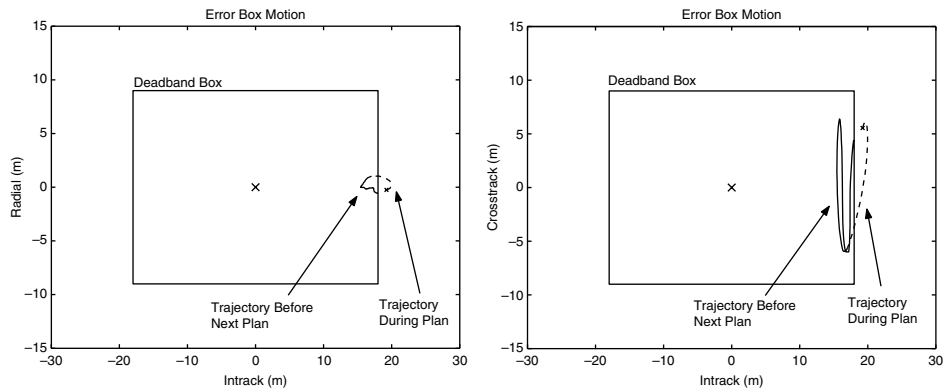

Fig. 8.11. Trajectory using unmodified terminal conditions.

1. The first imposes a fixed replan rate on the problem that is significantly shorter than the actual plan length. This is more typical of MPC algorithms than the variable replan length. Using this approach, replanning still forces the end of the planned trajectory to always be near the edge of the deadband. However, the high frequency of the replanning means that only the first few steps of a plan are ever implemented, so the spacecraft rarely reaches the edge of the box. This approach has the added advantage that it does not require as high a level of robustness, because the high feedback rate mitigates the effects of sensor noise.
2. A second approach retains the variable replan rate, but alters the terminal condition of the optimization. In the original problem, the terminal condition stated that the spacecraft should be guaranteed to finish the path inside the deadband. The new terminal condition specifies that the spacecraft should be guaranteed to end inside the deadband, but also that the nominal trajectory (i.e., the projected motion based on the nominal state estimate) should stay inside the error box for a full additional orbit, and that the terminal and initial states of that nominal motion must match. This new terminal condition is more restrictive than the original, but it can result in trajectories that drift for many (i.e., 5–12) orbits inside the deadband.

The second approach uses an alternate terminal condition and replaces the constraints in Eq. (8.44) with

$$\begin{aligned}
&\begin{bmatrix} \Gamma(k) & -\Gamma(k) \\ -\Gamma(k) & \Gamma(k) \end{bmatrix} \begin{bmatrix} U_k^+ \\ U_k^- \end{bmatrix} \leq \begin{bmatrix} z_{\text{des}}(k) - h_i(k) + z_{\text{tol}} \\ -z_{\text{des}}(k) + h_i(k) + z_{\text{tol}} \end{bmatrix} \forall \begin{matrix} k \in \{1, \ldots, n\} \\ i \in \{1 \ldots n_{\text{ic}}\} \end{matrix} \\
&\begin{bmatrix} \Gamma(n) & -\Gamma(n) \\ -\Gamma(n) & \Gamma(n) \end{bmatrix} \begin{bmatrix} U_n^+ \\ U_n^- \end{bmatrix} \leq \begin{bmatrix} z_{\text{des}}(j) - h_i(j) + z_{\text{tol}} \\ -z_{\text{des}}(j) + h_i(j) + z_{\text{tol}} \end{bmatrix} \forall \begin{matrix} j \in \{n+1, \ldots, n+q\} \\ i \in \{1, \ldots, n_{\text{ic}}\} \end{matrix}
\end{aligned} \tag{8.45}$$

and

$$\begin{bmatrix} (\bar{\Gamma}(n) - \Gamma(q)) & (\Gamma(q) - \bar{\Gamma}(n)) \end{bmatrix} \begin{bmatrix} U_q^+ \\ U_q^- \end{bmatrix} = \begin{bmatrix} h_{\text{nom}}(q) - h_{\text{nom}}(n) \end{bmatrix} \tag{8.46}$$

$$\begin{bmatrix} -I & 0 \\ 0 & -I \end{bmatrix} \begin{bmatrix} U_n^+ \\ U_n^- \end{bmatrix} \leq \begin{bmatrix} 0 \\ 0 \end{bmatrix} \tag{8.47}$$

where h_{nom} is the vector based on the nominal initial conditions (i.e., the current best state estimate), $\bar{\Gamma}(n)$ is $[\ \Gamma(n)^T \ \ 0_{1\times q}\ ]^T$, and q is the number of time steps beyond the end of the plan that the spacecraft is required to drift inside the error box. For the altered terminal conditions, q is set to the number of time steps in an orbit, to ensure the spacecraft remains in the error box without thrusting for a full orbit beyond the end of the thrusting plan. Because relative orbital dynamics (e.g., Hill's equations) are typically cyclic over the period of an orbit, an elliptical relative trajectory that remains inside the error box and begins and terminates at the same state is a nominal invariant terminal set [63]. Attaining this ideal terminal trajectory would preclude all future error box violations. However, no single state can be attained robustly in the presence of sensing noise and hence, the objective is made to *nominally* achieve the invariant trajectory while robustly satisfying the actual error box constraints.

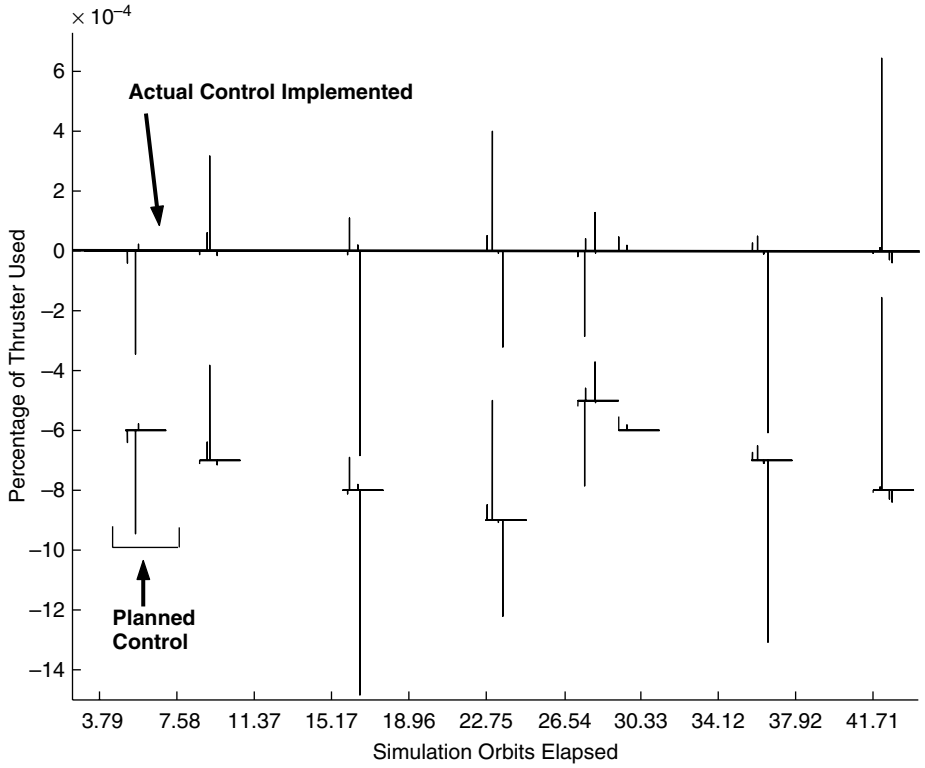

Fig. 8.12. Plans created using closed ellipse terminal conditions. The horizontal axis crossing the origin shows the thrusting that was implemented. The floating axes below the implementation axis indicate the planned thrusting sequence at time matching the far left side of each floating axis.

Figures 8.12 and 8.13 show the effect of changing the terminal condition. Both the frequent replan and altered terminal condition methods have similar fuel use rates. Interestingly, both tend to use slightly more fuel than the original problem in Ref. [59], which is likely a result of the more restrictive terminal conditions. However, when the terminal conditions were altered to create a closed-ellipse, the resulting spacecraft trajectories remained inside the error box without replanning, and consequently without control inputs, for much longer periods of time. This is a desirable condition, because the trajectory in Figure 8.13 now fills more of the error box and the spacecraft spends longer periods of time drifting. This both mitigates error introduced through thrusting and allows missions that can only collect science while drifting to utilize longer observation periods.

This section has examined the effects of terminal condition on the closed-loop behavior of a spacecraft formation with sensing noise. Ref. [12] showed that incorporating open-loop robustness into a formulation improved overall performance. Here, we demonstrated that the addition of a nominal terminal invariant set condition (i.e., the closed ellipse trajectory constraint) reduced the frequency with which replanning was required.

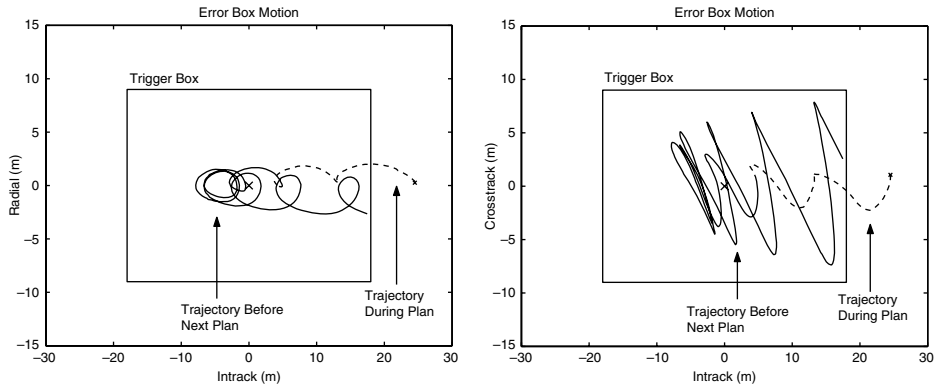

Fig. 8.13. Trajectory using closed ellipse terminal conditions.

Section 8.6, examines the comparative benefits of closed-loop robustness using a fixed replan rate and examines the application of the nominal closed ellipse condition in that formulation.

8.6 Using closed-loop robust MPC

Sensor noise in a spacecraft formation flying mission using carrier-phase differential GPS (CDGPS) will be a dominant disturbance [7]. Section 8.5 presents an approach to mitigating the effects of sensor noise on a model predictive control algorithm. This robustness was achieved by designing trajectories that would meet performance criteria for a set of possible initial conditions. The size of this set was determined by the expected sensor noise. The approach taken in that paper is characterized as "open-loop," because it generates a trajectory which is feasible for all initial conditions, without requiring replanning. An alternate approach is to design a thrusting plan which will be guaranteed to produce a feasible state and a new feasible plan at the next time step. This approach is considered "closed-loop," because each plan explicitly considers future feedback action in response to as-yet unknown information [64]. In contrast to the open-loop approach in Section 8.5, here it is desirable to use a fixed replanning rate, because the closed-loop approach exploits newly available information and must explicitly account for when that information will be available.

To demonstrate the feasibility of the robust model predictive control for actual spacecraft formation flight, a non-linear simulation with a realistic disturbance model is performed for multiple spacecraft over an extended period of time. We develop a formulation that simultaneously incorporates bounds on state error, process noise, sensor noise, and thrust availability. Simulations demonstrate the effectiveness of both the bounded models and of the closed-loop robustness technique applied to a realistic spacecraft formation control problem. The terminal conditions presented in [62] and others suggested in Section 8.5 are also examined.

8.6.1 Overview of robust MPC

For the spacecraft formation flying problem with sensor noise, robust feasibility guarantees that, provided the initial optimization is feasible and the noise is bounded, all subsequent optimizations are feasible and constraints are satisfied, e.g., the spacecraft remains inside the specified error box. This guarantee holds despite the plans being based on inaccurate information. References [17, 65] prove that the formulation reviewed in this section guarantees both robust feasibility and constraint satisfaction. Reference [63] describes an approach to transform the dynamics of the *true* state $\mathbf{x}$ to those of the *estimated* state $\hat{\mathbf{x}}$. This section assumes that an estimate of the true state is available and is equivalent to a linear combination of a bounded noise added to the true state. Robust feasibility depends on the estimate, since that is the initial condition parameter of the optimization. The dynamics of the true state are

$$\mathbf{x}(k+1) = \mathbf{F}\mathbf{x}(k) + \mathbf{G}\mathbf{u}(k) \tag{8.48}$$

and the estimation error is an additive term, applied at each time step

$$\hat{\mathbf{x}}(k) = \mathbf{x}(k) + \mathbf{n}(k) \tag{8.49}$$

$$\hat{\mathbf{x}}(k+1) = \mathbf{x}(k+1) + \mathbf{n}(k+1), \tag{8.50}$$

where $\mathbf{n}(k)$ is the navigation error at time k, which is assumed to lie in a bounded set $\mathcal{N}$. Substituting Eqs. (8.49) and (8.50) into Eq. (8.48) gives the dynamics of the estimate

$$\begin{aligned} \hat{\mathbf{x}}(k+1) &= \mathbf{F}\hat{\mathbf{x}}(k) + \mathbf{G}\mathbf{u}(k) + \mathbf{n}(k+1) - \mathbf{F}\mathbf{n}(k) \\ &= \mathbf{F}\hat{\mathbf{x}}(k) + \mathbf{G}\mathbf{u}(k) + \begin{bmatrix} -\mathbf{F} & \mathbf{I} \end{bmatrix} \begin{pmatrix} \mathbf{n}(k) \\ \mathbf{n}(k+1) \end{pmatrix}. \end{aligned} \tag{8.51}$$

With the dynamics now involving an affine disturbance, the formulation of [63] can be employed to synthesize a robustly feasible MPC algorithm. The disturbance vector is bounded using

$$\mathbf{w}(k) = \begin{bmatrix} -\mathbf{F} & \mathbf{I} \end{bmatrix} \begin{pmatrix} \mathbf{n}(k) \\ \mathbf{n}(k+1) \end{pmatrix} \in \mathcal{W} \quad \forall k. \tag{8.52}$$

If $\mathcal{N}$ is polyhedral, the set $\mathcal{W}$ is polyhedral and can therefore be generated using a polyhedral mapping routine of the form in Ref. [66]. Output constraints take the form

$$\mathbf{y}(k) = \mathbf{H}\hat{\mathbf{x}}(k) + \mathbf{J}\mathbf{u}(k) \in \mathcal{Y} \quad \forall k, \tag{8.53}$$

where $\mathcal{Y}$ is a bounded set which can incorporate error box and thrust constraints.

The MPC optimization is performed over a horizon of N steps and uses an arbitrary nilpotent linear control law $\mathbf{u}(j) = \mathbf{K}_{NP}\mathbf{x}(j)$ $j \in \{0 \ldots N-1\}$. Define $\mathbf{L}(j)$ as the state transition matrix for the closed-loop system under this control law

$$\mathbf{L}(0) = \mathbf{I} \tag{8.54}$$

$$\mathbf{L}(j+1) = (\mathbf{F} + \mathbf{G}\mathbf{K}_{NP})\,\mathbf{L}(j) \quad \forall j \in \{0 \ldots N\}. \tag{8.55}$$

Then the nilpotency requirement for $\mathbf{K}_{NP}$ implies

$$\mathbf{L}(N) = \mathbf{0}. \tag{8.56}$$

Define the MPC optimization problem $\mathsf{P}(\hat{\mathbf{x}}(k))$

$$J^*(\hat{\mathbf{x}}(k)) = \min_{\mathbf{u},\mathbf{x},\mathbf{y}} \sum_{j=0}^{N} \ell\left(\mathbf{u}(k+j|k), \mathbf{x}(k+j|k)\right), \tag{8.57}$$

subject to

$$\forall j \in \{0 \ldots N\}$$

$$\mathbf{x}(k+j+1|k) = \mathbf{F}\mathbf{x}(k+j|k) + \mathbf{G}\mathbf{u}(k+j|k) \tag{8.58}$$

$$\mathbf{y}(k+j|k) = \mathbf{H}\mathbf{x}(k+j|k) + \mathbf{J}\mathbf{u}(k+j|k) \tag{8.59}$$

$$\mathbf{x}(k|k) = \hat{\mathbf{x}}(k) \tag{8.60}$$

$$\mathbf{x}(k+N+1|k) \in \mathcal{X}_F \tag{8.61}$$

$$\mathbf{y}(k+j|k) \in \mathcal{Y}(j) \tag{8.62}$$

where the double subscript notation $(k+j|k)$ denotes the prediction made at time k of a value at time $k+j$. The constraint sets are chosen according to the recursion

$$\mathcal{Y}(0) = \mathcal{Y} \tag{8.63}$$

$$\mathcal{Y}(j+1) = \mathcal{Y}(j) \sim (\mathbf{H} + \mathbf{J}\mathbf{K}_{NP})\,\mathbf{L}(j)\mathcal{W} \quad \forall j \in \{0 \ldots N\} \tag{8.64}$$

where $\sim$ denotes the Pontryagin difference operation [67], defined by

$$\mathcal{X} \sim \mathcal{Y} \triangleq \{\mathbf{z} \mid \mathbf{z} + \mathbf{y} \in \mathcal{X}\ \forall \mathbf{y} \in \mathcal{Y}\} \tag{8.65}$$

and the matrix mapping of a set is defined such that

$$\mathbf{A}\mathcal{X} \triangleq \{\mathbf{z} \mid \exists \mathbf{x} \in \mathcal{X} : \mathbf{z} = \mathbf{A}\mathbf{x}\} \tag{8.66}$$

A MATLAB toolbox for performing these operations on polyhedral sets is available in Ref. [66, 68]. The choice of the terminal constraint $\mathcal{X}_F$ is typically very problem-specific. It must be a control invariant admissible set [68], i.e., there exists a control law $\boldsymbol{\kappa}(\mathbf{x})$ satisfying the following

$$\forall \mathbf{x} \in \mathcal{X}_F$$

$$\mathbf{F}\mathbf{x} + \mathbf{G}\boldsymbol{\kappa}(\mathbf{x}) \in \mathcal{X}_F, \tag{8.67}$$

$$\mathbf{H}\mathbf{x} + \mathbf{J}\boldsymbol{\kappa}(\mathbf{x}) \in \mathcal{Y}(N). \tag{8.68}$$

The origin $\mathcal{X}_F = \{\mathbf{0}\}$ is a straightforward choice of terminal set for a linear system. However, any nominally invariant set is valid for $\mathcal{X}_F$. Note that it is demonstrated in Subsection 8.6.3 that the origin can be an overly restrictive terminal condition for this control application.

8.6.2 Bounding the process noise

Section 8.5 describes an open-loop approach to accounting for disturbances in a model predictive control algorithm. This approach uses analytic models of J_2 and drag to predict time-varying disturbances which are then added to the LP formulation in Eq. 8.32. The closed-loop approach in Refs. [62, 63, 65] uses constant dynamics and a bounded disturbance model. The method for computing this model develops polytopic bounds on the disturbance set by simulating two spacecraft in close proximity to one another and propagating both using the high fidelity nonlinear integration-based propagator (NLP) and Hill's equations. The NLP used for the bounding process includes the perturbations due to J_2, drag, third body effects, and solar pressure. At each time step in the simulation propagates the previous state of the NLP forward using both a Hill's propagator and the NLP. The bounding method stores the magnitude of the difference between the two different states for both the position and the velocity states. The simulations use different initial starting states of the second satellite within an error box ($5 \times 10 \times 5$ m in the radial, in-track, and cross-track directions, respectively) centered about the first satellite. The maximum perturbations for position and velocity are found by calculating the absolute value of the differences between the nonlinear and linear propagated states from all of the simulations.

For a low Earth orbit (LEO) reference orbit ($n = 0.001$ rad/s), the disturbance sets for a 100 second propagation time step were found to be

$$\begin{pmatrix} p_x \\ p_y \\ p_z \end{pmatrix} \leq \begin{pmatrix} 85.5 \\ 30.3 \\ 0.0168 \end{pmatrix} \qquad \begin{pmatrix} v_x \\ v_y \\ v_z \end{pmatrix} \leq \begin{pmatrix} 0.635 \\ 0.323 \\ 0.00334 \end{pmatrix} \tag{8.69}$$

in units of centimeters and millimeters per second, respectively. These numbers are roughly on the same order of magnitude as the sensing noise, which is expected, given the large integration time step and the presence of many dynamic effects not modeled by Hill's equations. Another approach to developing a disturbance model of this type would be to use analytical models of the effects of J_2, drag, and nonlinearities to due separation distance and eccentricity. For a given reference orbit, the maximum perturbation predicted by each model would be combined to give the largest possible unmodeled disturbance on Hill's equations.

8.6.3 Controller implementation

To use the model predictive control formulation reviewed in Section 8.6.1, the system described in Eq. (8.48) is augmented with an additive disturbance, $\mathbf{q}(k)$, which will be used to represent process noise. The system in Eq. (8.48) then becomes

$$\mathbf{x}(k+1) = \mathbf{F}\mathbf{x}(k) + \mathbf{G}\mathbf{u}(k) + \mathbf{q}(k) \tag{8.70}$$

where $\mathbf{q}(k)$ in a vector belonging to a bounded polyhedral set $\mathcal{Q}$. Likewise, the estimated state with sensing noise in Eq. (8.51) becomes

$$\hat{\mathbf{x}}(k+1) = \mathbf{F}\hat{\mathbf{x}}(k) + \mathbf{G}\mathbf{u}(k) + \begin{bmatrix} -\mathbf{F} & \mathbf{I} & \mathbf{I} \end{bmatrix} \begin{pmatrix} \mathbf{n}(k) \\ \mathbf{n}(k+1) \\ \mathbf{q}(k) \end{pmatrix} \tag{8.71}$$

This altered formulation yields the new bounded disturbance set $\mathcal{W}$

$$\mathbf{w}(k) = \begin{bmatrix} -\mathbf{F} & \mathbf{I} & \mathbf{I} \end{bmatrix} \begin{pmatrix} \mathbf{n}(k) \\ \mathbf{n}(k+1) \\ \mathbf{q}(k) \end{pmatrix} \in \mathcal{W} \ \forall k. \tag{8.72}$$

The robust formulation in Section 8.6.1 can accommodate a disturbance set of this form, but its implementation is complicated by the high dimensionality of the uncertainty set and constraints. In particular, the calculation of the Pontryagin difference is the subject of on-going work. Therefore, an approximation is used, whereby two scalar noise inputs capture the dominant sensing uncertainty. This approximation is extended to represent sensing noise uncertainty in all states and a term is added to the to represent the process noise. The bounds on a single sensor noise $\mathbf{n}(k)$ are $\pm\mathbf{e}\bar{N}$. This constraint is unchanged if a new vector, $\mathbf{e}_{\text{sn}}$ is defined as

$$\mathbf{e}_{\text{sn}} = \bar{N}\mathbf{e} \tag{8.73}$$

and $\bar{n}(k)$ is now distributed over the bounded set

$$-1 \leq \bar{n}(k) \leq 1. \tag{8.74}$$

For the examples in this section, $\mathbf{e}_{\text{sn}}$ is defined to be the expected noise on relative spacecraft states in a CDGPS system: 0.02 meters for position sensing and 0.0005 m/s for velocity sensing.

A vector, $\mathbf{e}_{\text{pn}}$, describing the maximum process noise magnitude on each state (taken directly from Eq. (8.69)) is introduced to form an approximation for the total possible state perturbation due to noise at any step k. The disturbance vector $\mathbf{w}(k)$ is now defined to be

$$\mathbf{w}(k) = \begin{bmatrix} (\mathbf{e}_{\text{pn}} - \mathbf{F}\mathbf{e}_{\text{sn}}) & \mathbf{e}_{\text{sn}} \end{bmatrix} \begin{pmatrix} \bar{n}(k) \\ \bar{n}(k+1) \end{pmatrix} \in \overline{\mathcal{W}} \quad \forall\, k. \tag{8.75}$$

The new set $\overline{\mathcal{W}}$ attempts to capture the uncertainty present in the formation flying demonstrations conducted in this section. Current research is investigating computationally efficient methods of accurately bounding the actual $\mathcal{W}$.

8.6.4 Demonstration results

The demonstration of closed-loop robustness in this section incorporates the error box concept from Section 8.3 and the virtual center concept for coordination from Section 8.4. In addition, the effect of the nominal closed-ellipse constraint from Section 8.5 is also

examined. The demonstration is done using a nonlinear orbit propagator [60] with realistic disturbance and sensor noise models.

In this demonstration, the output constraints on each spacecraft will be both on the spacecraft state and on the input magnitude. The spacecraft state will be constrained to error box of dimensions (in meters) of $5 \times 10 \times 5$ in the radial, in-track, and cross-track directions, respectively, of an LVLH frame. In addition, the spacecraft will be constrained to have a maximum acceleration in each direction of 0.003 m/s^2. The cost function will be the one-norm of the thrust inputs over the planning horizon. The controller's cost function and constraints are both linear, so the controller optimizations are formulated as linear programs. A two week simulation of four spacecraft on an equally spaced passive aperture formation is shown in Figure 8.14. The passive aperture formation is a drift-free in-track–cross-track projected circle with a 100 meter radius and in-track–radial 400×200 m ellipse. The "tube" of spacecraft trajectories is essentially the error boxes in Figure 8.3 moving around the relative trajectory of the formation. The fuel-weighted virtual center method described in Section 8.4, is used to minimize state error and equalize fuel use across the formation. Spacecraft error box motion throughout the duration of the simulation is shown in Figure 8.17. It can be observed from the figures that no spacecraft exceeds its state constraints at any time in the simulation. However, the trajectories of the spacecraft remained close to the center of their respective error boxes, likely a result of the requirement that the each spacecraft arrive at the origin at the end of its plan. On average over the course of the simulation, each spacecraft used 14.5 mm/s of fuel

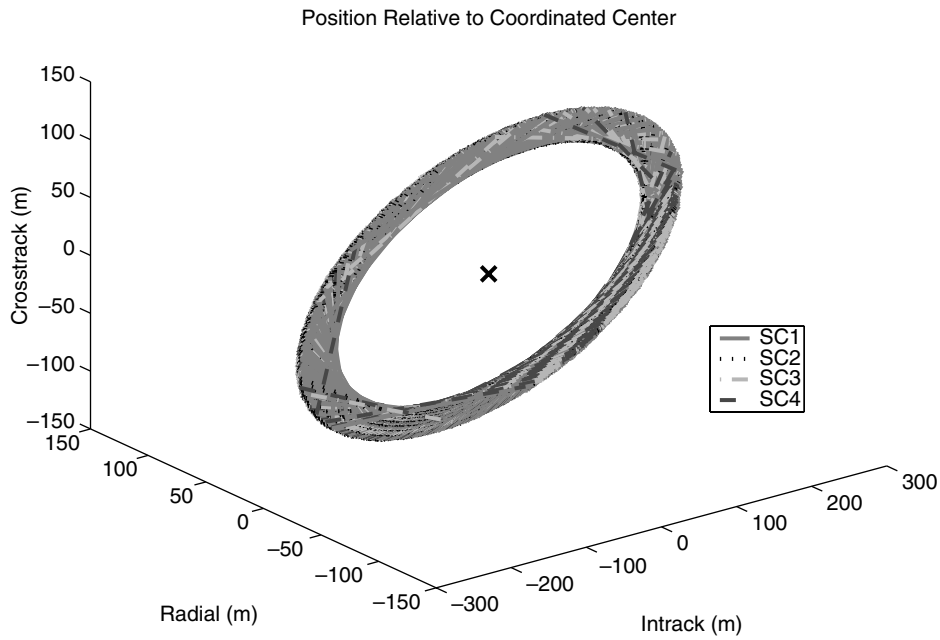

Fig. 8.14. Formation relative to the virtual center.

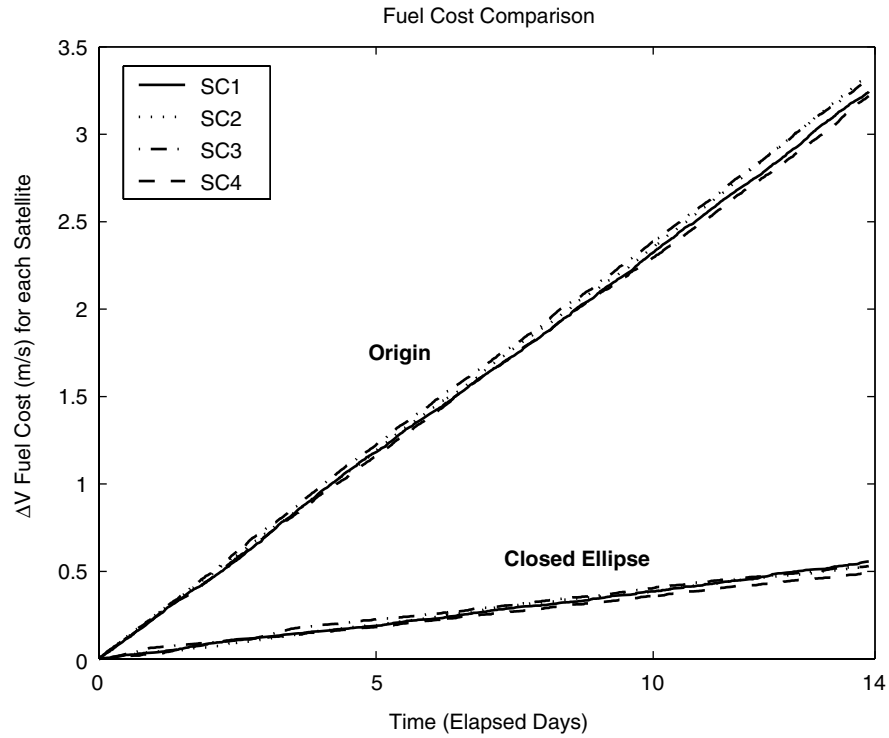

Fig. 8.15. Effect of terminal condition on fuel use rates.

per orbit, significantly more than 2.46 mm/s per orbit, the value reported for a similar simulation in Ref. [16].

These fuel expenditures can be reduced using the closed-ellipse constraint from Section 8.5 that restrict the spacecraft to terminate their plans on a closed ellipse in the LVLH frame. This requirement is enforced through two conditions:

1. The spacecraft must remain inside the error box at every time step for a full orbit after the plan ends.
2. The spacecraft state at the end of the plan is restricted to be the same as the state a full orbit after the end of the plan.

The origin terminal condition is a subset of the closed form ellipse terminal condition, because Hill's equations state that a spacecraft at the origin of an LVLH frame (i.e., zero position and zero velocity) will remain motionless in that frame. This motionless trajectory is a closed form ellipse with major and minor radii of zero meters. The difference between the terminal conditions is illustrated in Figure 8.16.

Figure 8.18 shows error box motion during a two week simulation using the closed ellipse terminal conditions. It is clear that the spacecraft motion occupies a much larger region of the error box and appears to take on the shape of an ellipse in the in-track–radial plane. As expected, the less restrictive terminal conditions led to significantly

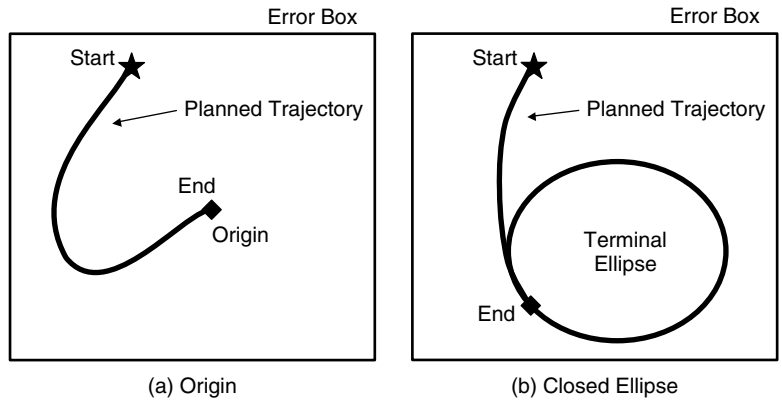

Fig. 8.16. Terminal conditions examined for closed loop MPC.

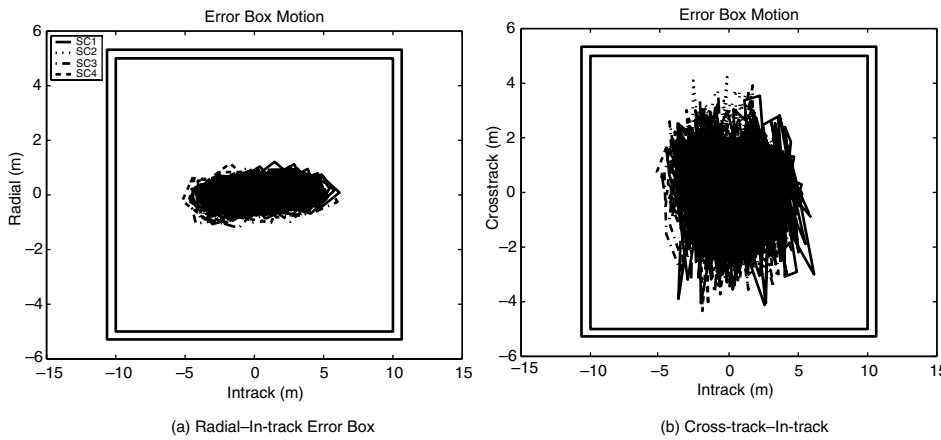

Fig. 8.17. Error box motion using Origin terminal constraint.

lower average fuel usage: 2.22 mm/s per orbit, which is a slight improvement over the results in Ref. [16]. Figure 8.15 compares the fuel use rates of a four spacecraft formation over a two week period. In contrast to the approach used in Section 8.5, the closed-loop robust method replans at all times, effectively guaranteeing that the spacecraft never drifts out of the error box. Furthermore, the spacecraft never enters an area of the error box that would be costly, from a fuel-use perspective, to prevent a constraint violation. The tradeoff for using the closed-loop method is that known time-varying disturbances must now be modeled as bounded polytopes, which does not allow the controller to fully exploit the well-known orbital dynamics. It is likely that performance can be further improved by using the LTV relative dynamics used for planning in Ref. [56] (excluding

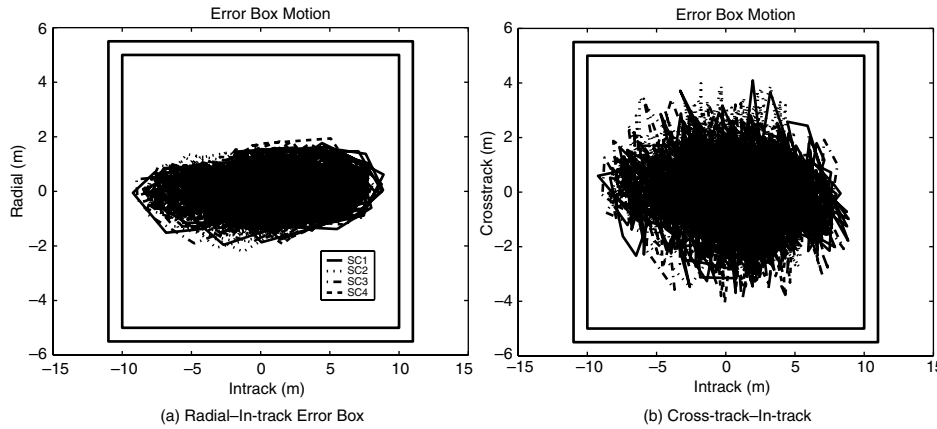

Fig. 8.18. Error box motion using Closed Ellipse terminal constraint.

cross disturbances) to capture J_2 effects and creating a new bounded process noise model. By including some of the effects of J_2 in the state transition matrix, the system should be better able to exploit natural dynamics and be capable of operating with less conservative process noise bounds. Both of these improvements should reduce overall fuel use.

Spacecraft formation flying simulations using the closed loop MPC controller were conducted in a realistic environment using realistic constraints. These simulations incorporated cooperation through the virtual center technique and a nominal terminal invariant set through the closed-ellipse technique. Results of these simulations show that the techniques can be used to control spacecraft for long periods of time reliably (i.e., no constraint violations) and with low fuel use.

8.7 Conclusions

This chapter developed three modifications to a basic formation flying model predictive control system to improve practical implementation. First, the virtual center method enabled cooperation between satellites by using a weighted optimization to find the optimal formation reference point. The addition of an feasible ellipse terminal constraint to an open-loop robust MPC formulation was demonstrated to reduce the frequency of required replanning, a desirable characteristic in an open-loop planning scheme. An alternate closed-loop robustness approach using fixed-rate replanning was extended to the formation flying control problem and was shown to be fuel efficient and capable of using virtual center fleet cooperation and the closed-ellipse terminal condition robustly. Several high-fidelity nonlinear simulations demonstrated all three modifications in use simultaneously to robustly and efficiently control a three satellite formation over a two week period in the presence of realistic disturbances and sensor noise.

8.8 Nomenclature

CDGPS—Carrier-Phase Differential GPS
GN&C—Guidance, Navigation, and Control
GPS—Global Positioning System
GVEs—Gauss' Variational Equations
LEO—Low Earth Orbit
LP—Linear Program
LPV—Linear Parameter-Varying
LTI—Linear Time Invariant
MPC—Model Predictive Control
NLP—Nonlinear Propagator
SMA—Semimajor Axis
ZOH—Zero Order Hold

Acknowledgments

The authors would like to acknowledge Dr. Arthur Richards for his insights into the design of a computationally tractable closed-loop robust MPC. This work was funded under Air Force Grant F49620-99-1-0095, NASA Grant #NAG5-10440, and Cooperative Agreement NCC5-729 through the NASA GSFC Formation Flying NASA Research Announcement. Any opinions, findings, and conclusions or recommendations expressed in this material are those of the author(s) and do not necessarily reflect the views of the National Aeronautics and Space Administration.

References

1. Bauer, F.H., Hartman, K., Bristow, J., Weidow, D., How, J.P. and Busse F. (1999). Enabling spacecraft formation flying through spaceborne GPS and enhanced autonomy technologies. *ION-GPS '99*, Proceedings of the *12th International Technical Meeting of the Satellite Division of the Institute of Navigation*, Sept. 14–17, pp. 369–383.
2. Leitner, J., Bauer, F., Folta, D., Moreau, M., Carpenter, R. and How, J. (2002). Distributed Spacecraft Systems Develop New GPS Capabilities, in *GPS World: Formation Flight in Space*, Feb. 2002.
3. The MAXIM Mission (2005). Online at http://maxim.gsfc.nasa.gov, last accessed Nov. 2005.
4. The Stellar Imager Mission (2005). Online at http://hires.gsfc.nasa.gov/si/ last accessed Nov. 2005.
5. The Terrestrial Planet Finder mission (2005). Online at http://tpf.jpl.nasa.gov last accessed Nov. 2005.
6. Carpenter, J.R., Leitner, J.A., Folta, D.C. and Burns, R.D. (2003). Benchmark Problems for Spacecraft Formation Flying Missions. AIAA *Guidance, Navigation and Control Conference*, Austin, TX, AIAA-5364.
7. How, J.P. and Tillerson, M. (2001). Analysis of the Impact of Sensor Noise on Formation Flying Control. *Proc. of the American Control Conf.*, June, pp. 3986–3991.
8. Carpenter, R. and Alfriend, K. (2003). Navigation accuracy guidelines for orbital formation flying. *Proceedings of the AIAA Guidance Navigation and Control Conference*, Austin, TX, August 11–14.
9. Alfriend, K.T. and Lovell, T.A. (2003). Error Analysis of Satellite Formations in Near-Circular Low-Earth Orbits. (AAS 03-651), Vol. 116, Advances in the Astronautical Sciences.
10. Scharf, D., Ploen, S. and Hadaegh, F. (2003). A Survey of Spacecraft Formation Flying Guidance and Control (Part I): Guidance. *IEEE American Control Conference*, June.

11. Scharf, D., Hadaegh, F. and Ploen, S. (2004). A Survey of Spacecraft Formation Flying Guidance and Control (Part II): Control. *IEEE American Control Conference*, June, 2976–2985.
12. Tillerson, M., Inalhan, G. and How, J. (2002). Coordination and Control of Distributed Spacecraft Systems Using Convex Optimization Techniques. *International Journal of Robust and Nonlinear Control*, **12**(2–3), pp. 207–242.
13. Melton, R.G. (2002). Time explicit representation of relative motion between elliptical orbits. *Journal of Guidance, Control, and Dynamics*, **23**(4), pp. 604–610.
14. Breger, L.S., Ferguson, P., How, J.P., Thomas, S., McLoughlin, T. and Campbell, M. (2003). Distributed control of formation flying spacecraft built on OA. Presented at the AIAA *Guidance, Navigation and Control Conference*, August.
15. Gim, D.W. and Alfriend, K.T. (2003). State transition matrix of relative motion for the perturbed noncircular reference orbit. *AIAA Journal of Guidance, Control, and Dynamics*, **26**(6), pp. 956–971.
16. Tillerson, M., Breger, L.S. and How, J.P. (2003). Multiple spacecraft coordination & control. Presented at the *American Control Conference*, June, pp. 1740–1745.
17. Richards, A.G. and How, J.P. (2005). A computationally-efficient technique for robust model predictive control, submitted to IEEE *Transactions on Automatic Control*, Feb. 2005.
18. Hill, G.W. (1878). Researches in Lunar Theory, *American Journal of Mathematics*, **1**, pp. 5–26, 129–147, 24–260.
19. Lawden, D. (1963). *Optimal Trajectories for Space Navigation*, Butterworths, London.
20. Carter, T. (1990). New form for the optimal rendezvous equations near a keplerian orbit. *AIAA Journal of Guidance, Control, and Dynamics*, **13**, pp. 183–186.
21. Inalhan, G., Tillerson, M. and How, J.P. (2002). Relative dynamics and control of spacecraft formations in eccentric orbits. *AIAA JGCD*, **25**(1), pp. 48–59.
22. Marec, J. (1979). *Optimal Space Trajectories* Elsevier Scientific, NY.
23. Battin, R.H. (1987). *An Introduction to the Mathematics and Methods of Astrodynamics*, AIAA Education Series, New York.
24. Bate, R., Mueller, D. and White, J. (1971). *Fundamentals of Astrodynamics*, Dover Publications Inc., NY.
25. Chobotov, V. (1996). *Orbital Mechanics*. Second Edition, AIAA Educational Series.
26. Schweighart, S. (2001). *Developement and Analysis of a High Fidelity Linearized J2 Model for Satellite Formation Flying*, S.M. Thesis, Massachusetts Institute of Technology, Dept. Aeronautics and Astronautics, June.
27. Karlgrad, C.D. and Lutze, F.H. (2002). Second order relative motion equations. *Advances in the Astronautical Sciences*, **109**, Pt. 3, 202, pp. 2429–2448.
28. Gim, D.T. and Alfriend, K.T. (2003). State Transition Matrix of Relative Motion for the Perturbed Noncircular Reference Orbit, *Journal of Guidance, Control and Dynamics*, **26**(6), pp. 956–971.
29. Mitchell, J.W. and Richardson, D.L. (2003). A third order analytic solution for relative motion with a circular reference orbit. *Journal of the Astronautical Sciences*, **51**(1), pp. 1–12.
30. Alfriend, K.T. and Yan, H. (2005). Evaluation and comparison of relative motion theories. *Journal of Guidance, Control and Dynamics*, **28**(2), pp. 254–261.
31. Alfriend, K.T., Schaub, H. and Gim, D.W. (2002). Formation flying: accomodating non-linearity and eccentricity perturbations. Presented at the 12th *AAS/AIAA Space Flight Mechanics Meeting*, January 27–30.
32. Breger, L.S. and How, J.P. (2004). GVE-based dynamics and control for formation flying spacecraft. Presented at the *2nd International Formation Flying Symposium*, September.
33. Breger, L.S. and How, J.P. (2005). J_2-modified GVE-based MPC for formation flying spacecraft. Presented at the *AIAA Guidance, Navigation and Control Conference*, August.
34. Kapila, V., Sparks, A.G. Buffington, J.M. and Yan, Q. (1999). Spacecraft formation flying: dynamics and control. *American Control Conference*, San Diego, CA, June 2–4, Institute of Electrical and Electronic Engineers, pp. 4137–4141.
35. Ren, W. and Beard, R. (2002). Virtual structure based spacecraft formation control with formation feedback. *AIAA GN&C Conference*, August.
36. Mishne, D. (2002). Formation control of LEO satellites subject ot drag variations and J_2 perturbations. *AAS/AIAA Astrodynamics Specialist Conference*, Monterey, CA, August.
37. Gurfil, P. (2003). Control-theoretic analysis of low-thrust orbital transfer using orbital elements. *AIAA Journal of Guidance, Control, and Dynamics*, **26**(6), November–December, pp. 979–983.

38. Schaub, H. and Junkins, J.L. (2003). *Analytical Mechanics of Space Systems*, AIAA Education Series, Reston, VA.
39. Naasz, B. (2002). *Classical Element Feedback Control for Spacecraft Orbital Maneuvers*, S.M. Thesis, Dept. of Aerospace Engineering, Virginia Polytechnic Institute and State University, May.
40. Yan, Q., Yang, G., Kapila, V. and de Queiroz, M. (2000). Nonlinear Dynamics and Output Feedback Control of Multiple Spacecraft in Elliptical Orbits. *Proceedings of 2000 American Control Conference*, Chicago, IL, June 28–30, **2** (A01-12740 01-63), Piscataway, NJ, Institute of Electrical and Electronics Engineers, pp. 839–843.
41. de Queiroz, M., Yan, Q., Yang, G. and Kapila, V. (1999). Global output feedback tracking control of spacecraft formation flying with parametric uncertainty. IEEE Conference on Decision and Control, 38th, Phoenix, AZ, Dec. 7–10, 1999, Proceedings. **1** (A00-4816014-63), Piscataway, NJ, Institute of Electrical and Electronics Engineers, Inc., pp. 584–589.
42. Sedwick, R., Miller, D. and Kong, E. (1999). Mitigation of differential perturbations in clusters of formation flying satellites, *Proceedings of the AAS/AIAA Space Flight Mechanics Meeting*, Breckenridge, CO, Feb. 7–10, 1999. Pt. 1 (A99-39751 10-12), San Diego, CA, Univelt, Inc. (Advances in the Astronautical Sciences. Vol. 102, pt. 1), pp. 323–342.
43. Schaub, H. and Alfriend, K. (1999). J_2 Invariant relative orbits for spacecraft formations. In *Goddard Flight Mechanics Symposium*, May 18–20, Paper No. 11.
44. Schaub, H. and Alfriend, K. (2001). Impulsive feedback control to establish specific mean orbit elements of spacecraft formations. *AIAA Journal of Guidance, Control, and Dynamics*, **24**(4), July–August, pp. 739–745.
45. Vadali, S., Vaddi, S., Naik, K. and Alfriend, K.T. (2001). Control of Satellite Formations, *Proceedings of the AIAA Guidance, Navigation, and Control Conference*, Montreal, Canada, August 6–9. AIAA Paper 2001-4028.
46. Sparks, A. (2000). Satellite formationkeeping control in the presence of gravity perturbations, *Proceedings of the 2000 American Control Conference*, Chicago, IL, June 28–30, 2000, **2** (A01-12740 01-63), Piscataway, NJ, Institute of Electrical and Electronics Engineers, pp. 844–848.
47. Redding, D., Adams, N. and Kubiak, E. (1989). Linear-quadratic stationkeeping for STS orbiter. AIAA *Journal of Guidance, Control, and Dynamics*, **12**, March–April, pp. 248–255.
48. Maciejowski, J.M. (2002). *Predictive Control with Constraints*, Prentice Hall.
49. Kwakernaak, H. and Sivan, R. (1972). *Linear Optimal Control Systems*, Wiley-Interscience.
50. Broucke, R.A. (2003). Solution of the elliptic rendezvous problem with the time as an independent variable. *AIAA Journal of Guidance, Control, and Dynamics*, **26**, July–August, pp. 615–621.
51. Franklin, G., Powell, J. and Workman, M. (1998). *Digital Control of Dynamic Systems*. Third Edition, Addison-Wesley.
52. Vallado, D. (1997). *Fundamentals of Astrodynamics and Applications*. McGraw-Hill.
53. Das, A. and Cobb, R. (1998). TechSat 21—Space missions using collaborating constellations of satellites. *Proceedings of AIAA/USU Annual Conference on Small Satellites*, 12th, Utah State University, Logan, August 31–September 3, 1998, Proceedings (A99-10826 01-20), Logan, UT, Utah State University.
54. Curtis, S. (1999). The Magnetospheric Multiscale Mission Resolving Fundamental Processes in Space Plasmas, NASA GSFC, Greenbelt, MD, December, NASA/TM2000-209883.
55. Bertsimas, D. and Tsitsiklas, J.N. (1997). Introduction to Linear Optimization, Athena Scientific, Belmont.
56. Tillerson, M. (2002). *Coordination and Control of Multiple Spacecraft using Convex Optimization Techniques*, S.M. Thesis, Dept. of Aeronautics and Astronautics, MIT, June.
57. Busse, F.D. and How, J.P. (2002). Real-time experimental demonstration of precise decentralized relative navigation for formation-flying spacecraft. *AIAA GNC*, August, Paper 2002–5003.
58. Busse, F.D. and How, J.P. (2002). Four-vehicle formation flying hardware simulation results. Presented at the *ION-GPS Conference*, September.
59. Inalhan, G., Tillerson, M. and How, J.P. (2002). Relative Dynamics & Control of Spacecraft Formations in Eccentric Orbits. *AIAA Journal of Guidance, Navigation, and Control*, **25**(1), pp. 43–53.
60. Solutions, A.I. (1999). *FreeFlyer User's Guide*. Version 4.0, March.
61. Tillerson, M. and How, J.P. (2002). Advanced guidance algorithms for spacecraft formation flying. Presented at the *American Control Conference*, May 2002, pp. 2830–2835.
62. Breger, L.S., Richards, A. and How, J.P. (2005). Model predictive control of spacecraft formations with sensing noise. Presented at the IEEE *American Control Conf.*, June, pp. 2385–2391.

63. Richards, A.G. and How, J.P. (2003). Model predictive control of vehicle maneuvers with guaranteed completion time and robust feasibility. *Proceedings of the American Control Conference*, June, pp. 4034–4040.
64. Scokaert, P.O.M. and Mayne, D.Q. (1998). Min-max feedback model predictive control for constrained linear systems. *IEEE Transactions on Automatic Control*, **43**(8), August, p. 1136.
65. Richards, A.G. and How, J.P. (2004). Robust constrained model predictive control with analytical performance prediction. Presented at the *AIAA Guidance, Navigation and Control Conf.*, Aug 2004. AIAA-2004-5110.
66. Kerrigan, E.C. (2003). Invariant Set Toolbox for Matlab, available at http://www-control.eng.cam.ac.uk/eck21, July.
67. Kolmanovsky, I. and Gilbert, E.G. (1995). Maximal Output Admissible Sets for Discrete-Time Systems with Disturbance Inputs. IEEE *American Control Conference*.
68. Kerrigan, E.C. (2000). Robust Constraint Satisfaction: Invariant Sets and Predictive Control. PhD Thesis, Cambridge University, November.